STUDIA

UNIVERSITATIS BABEŞ-BOLYAI

PHYSICA

1

1991

CLUJ-NAPOCA

ANUL XXXVI 1991

STUDIA

UNIVERSITATIS BABEŞ-BOLYAI

PHYSICA

1

Redacţia 3400 CLUJ-NAPOCA, str M Kogălniceanu 1, Telefon ● 11 61 01

SUMAR — CONTENTS — SOMMAIRE

STUDIA UNIV. BABEŞ-BOLYAI, PHYSICA, XXXVI, 1, 1991

A RAMAN STIMULATED BACKSCATTERING FEL ANALYSIS I.

SPERANŢA COLDEA*

ABSTRACT. The Free Electron Laser (*FEL*) is a feasible radiation source over a broad spectrum from millimeter to optical wavelength A simplified analysis based upon a linear theory is presented in the first part of this work, for the Raman regime *FEL* process The two parts of the paper discuss a type of a *FEL* which is based on the stimulated Raman backscattering of a magnetostatic, pump wave from a cold, dense, relativistic electron beam The results of a non-linear theory of the Raman *FEL* will be discussed in the second part of this work

1 **Introduction.** The conventional lasers are troubled by lack of energy storage, highly selective level excitation and low efficiency Several far infrared lasers have achieved an output power of 1 *MW*, as an exemple being the CH_3F-system which radiates at 496μ, Raman-like The conventional lasers present a narrow, stable line-width and excitation of just one (or a few) cavity modes Compared with the classic lasers the FELs are not only tunable radiation sources but could be used as amplifiers In a FEL, the bandwidth for positive gain is very large and many cavity modes are excited. The FEL systems are very sensitive to the fluctuation in the electron beam energy.

The linear and non-linear theories have been developed for two regimes of the FEL operation [1] — [12] for a monoenergetic electron beam in the Compton regime, where the space charge effects are neglected, and in the Raman regime, where the space charge effects are considerable.

The inclusion of these effects in the FEL simulation have been made in one-dymensional analysis [13] — [14] The usual general linear theory will be not presented here but a simplified discussion of the Raman regime FEL interaction will be done.

2. **The analysis of the Raman regime FEL operation.** The FEL dispersion relation obtained from a linear theory of the relativistic electron beam and a static hellically polarized wiggler field interaction [15] is of the general form:

$$\left[k - \left(\frac{\omega^2}{c^2} - F \cdot \frac{\omega_b^2}{\gamma_0 c^2}\right)^{1/2}\right] \cdot \left[\left(k + k_\omega - \frac{\omega}{v_{z0}}\right)^2 - \frac{\omega_b^2}{v_{z0}^2 \gamma_0 \gamma_z^2}\right] = -F \cdot \frac{\omega_b^2/c^2}{2\gamma_0} \beta_\omega^2 \beta_{z0}^{-3} k_\omega \tag{1.1}$$

where $\omega_b^2 = 4\pi ne^2/\gamma_z m$, $F = \sigma_b/\sigma_R$ is the filling factor associated with the radiation field (σ_b and σ_R being the cross-sections-areas of the electron and radiation beams), $\gamma_0 = \gamma_z \left[1 + (e/A_\omega/m_0c^2)^2\right]^{1/2}$, with $\gamma_z = (1 - v_{z0}^2/c^2)^{-1/2}$ being the

* *Department of Physics, University Babeş-Bolyai, 3400 Cluj-Napoca, Romania.*

relativistic factor of the electron beam and $\vec{A}_\omega$-the wiggler field, in the case when $|\vec{A}_\omega| >> |\vec{A}_R|$, $\vec{A}_R$ being the radiation filed

In the Raman regime, the beam-plasma frequency is sufficiently high that the coupling between the electromagnetic wave and the two beam waves can be considered independently The two beam vawes correspond to the negative and positive energy modes which could be described by a special dispersion relation for their interaction The effect of the positive energy beam mode on the coupling is weak and in this case $\{k - [\omega - v_{z0} \quad k_\omega + + \omega_b/(\gamma_z\sqrt{\gamma_0})/v_{z0}\}$ is replaced by $+ 2\omega_b/(\gamma_z v_{z0}\sqrt{\gamma_0})$ in the dispersion relation.

$$\left[k - \left(\omega^2 - F \cdot \frac{\omega_b^2}{\gamma_0}\right)^{1/2}/c\right] \cdot \left\{k - \left[\omega + v_{z0}k_\omega + \frac{\omega_b}{\gamma_z\sqrt{\gamma_0}}\right]/v_{z0} = \right.$$

$$= -\alpha^2 \quad \gamma_z \quad \gamma_0^{1/2} v_{z0}/2\omega_b \tag{1.2}$$

where

$$\alpha^2 = F\left(\frac{\omega_b^2}{2\gamma_0 c^2}\right) \beta_\omega^2 \cdot \beta_{z0}^{-2} \cdot k_\omega \tag{1 3}$$

The maximum Raman growth rate occurs when $k_m = k$, i e.

$$(\omega^2 - F \quad \omega_b^2/\gamma_0)^{1/2}/c = k_\omega$$

and has the folowing form.

$$\Gamma = Im\omega = \beta_\omega F^{1/2} \cdot \left(\frac{\omega_b \quad \gamma_z k_\omega}{4\sqrt{\gamma_0 c}}\right)^{1/2} \tag{1 4}$$

This is possible only if:

$$\beta_\omega \ll \beta_{crit} \tag{1 5}$$

where

$$\beta_{crit} = F^{-1/2} \quad (2\omega_b c^2/v_{z0}^3 \gamma_0^{1/2} \cdot \gamma_z^3 k_\omega)^{1/2} \tag{1 6}$$

For the Compton regime (high-gain) FEL interaction the condition is the reverse of the equation (1 5)

$$\beta_\omega \gg \beta^{crit} \tag{1 7}$$

The Raman regime could be distringuished from the Compton regime by defyning a critical beam-plasma density

$$\omega_{b,crit} = F\left(\frac{v_{z0}}{c}\right)^2 \quad \sqrt{\gamma_0}\, \gamma_z^3 \beta_\omega^2 v_{z0} k_\omega/2 \tag{1 8}$$

If $\omega_b \gg \omega_{b,crit}$ the FEL is in a Raman regime, if $\omega_b \ll \omega_{b,crit}$ the FEL operates in high-gain Compton regime

If a stimulated backscattering Raman proces (SRB) is considered (a parametric instability) in a magnetostatic pump field and a cold, dense, relativistic electron beam system, a detailed analysis of such a FEL interaction can be made The Stimulated Raman FEL is a system, in which an electron plasma (longitudinal) wave mode and an electromagnetic scattered mode feed on the energy of the pump with frequency ω_0. This type of FEL uses such

a convective instability which can amplify an electromagnetic signal Such a device can operate in three ways

(a) as an amplifier for noise (the superradiant model),
(b) as an amplifier for a coherent signal, and
(c) as an oscillator

We will develop a simplified analysis for the case of a SRB — FEL amplifier for a coherent signal

The result of the simplified linear dispersion relation of the FEL interaction is the solution for the real part of this equation giving the backscattering frequency or the stimulated backscattered mode wavelength.

$$\omega_s = \frac{\omega_0 - \omega_b/\gamma_z}{(1 - \beta_z)} \sim 2\gamma_z^2 \cdot \omega_0 \tag{1 9a}$$

and

$$\lambda_s = 1/2\gamma_z^2 \tag{1 9b}$$

with $\omega_0 = 2\pi\beta_\omega c/l = 2\pi v/l$ and $\beta_\omega = v_{z0}/c$

In the small signal approximation and weak pump regime the backscattered wave will grow exponentially along the rippled region of the magnetostatic field (wiggler or undulator field) The simplified growth rate obtained from eq. (1 2) — (1 4) is of the form.

$$\Gamma = Im\omega = \left(\frac{\omega_b}{\gamma_z\gamma_0}\right)^{1/2} \cdot \omega_\perp = \left(\frac{\omega_b}{4\pi\gamma_z}\frac{1}{c^3}\right)^{1/2} \cdot \tag{1 10}$$

where $\omega_\perp = eB_\perp/mc$ is related to the pump amplitude $B_\perp$.

As a matter of fact, there is another collective mode of the electron beam-the cyclotron instability which is a transverse mode, with the frequency given by

$$\omega_c = \frac{\omega_0 - \Omega_c/\gamma_z}{(1 - \beta_z)} \tag{1 11}$$

where $\Omega_c = eB_{z0}/mc$

In the situations where there is an inhomogeneity of the pump amplitude, transverse to the B_{z0} field there develops a space charge oscillation at the frequency Ω_c, which is driven by the ponderomotive force of the pump field and the scattered Raman wave. It is possible to show how the gain of the space charge mode varies with the beat frequency between the pump and signal waves When this beat is at the frequency ω_b the gain is very large, having a stimulated Raman emission (a Stokes mode) When the beat is at $-\omega_b$ we have a stimulated Raman absorbtion (an antiStokes mode) There is some gain due to the finite-length—two-wave beat in off-three-waves resonance case However, the net gain for the FEL laser system off-three-waves resonance is negative [16] The three-waves resonance has a finite bandwidth characteristic to the parametric processes $\Delta\omega_s \sim Im\omega$ Usually the efficiency of a FEL device is bounded by a pump depletion phenomenon, but the non-linear saturation mechanism in the FEL s will influence this efficiency (when the beam

fluctuation amplitude $\delta\eta \sim n$, which is the beam density) In the considered case the efficiency will be.

$$\eta \sim \frac{\omega_b}{2\omega_0\gamma_z} \sim 5\% \tag{1.12}$$

There is a distinction between the efficiency of the laser and of the amplifier: if one limits the efficiency to energy conversion for a single, this mode is given by:

$$\eta \sim \left(\frac{\omega_b}{8\gamma_z\omega_0}\right)^{1/2} \cdot \left|\frac{\omega_\perp}{\gamma_z\omega_0}\right| \sim 1\% \tag{1.13}$$

The laser has less efficiency than the amplifier, but the laser oscillators have other interesting properties, like the frequency stability

3 **Conclusions.** Other theories have uncovered some interesting effects: it was found that the span of the unstable wavenumber is very broad for high amplitude pump and high relativistic factors γ_z, high density electron beam [17] Theoretically, one might expect high gain Raman FEL amplifiers But when two-dimensional effects are considered in a numerical discussion [18] another difficulty occurs the stimulated Raman forwardscattering appears at a sufficiently high pump amplitude and long wiggler, as a low frequency absolute instability, which can grow to high amplitude and destroy the back-scattering process

Some comments upon the effects of the finite beam energy spread on the gain, could be made Excitation of the collective beam mode occurs only if the scattered wavelength exceeds the Debye length of the beam ($\lambda_s > \lambda_D$) and this fact requires a condition on the parallel beam energy spread.

$$\left(\frac{\Delta\gamma_z}{\gamma_z}\right)_{||} < \frac{1}{2} \cdot \frac{1}{\gamma_z}\left(\frac{\omega_b}{\omega_0}\right) \tag{2 1}$$

If this condition is not true, the gain is reduced an order of magnitude

$$\Gamma = Im\ \omega \approx \frac{\omega_b}{\omega_s} \cdot \frac{\omega_\perp^2}{(k_0 + k_s)^2} \cdot \frac{1}{v_{th}^2} \tag{2 2}$$

where v_{th} is the spread of electrons' energies $v_{th} = c\left(\frac{\Delta\gamma_z}{\gamma_z}\right)_{||}\gamma_z^{-2}$ The relation (2 2) is the stimulated Compton gain result

The influence of the beam energy spread on two- and three-wave lasers consists in a decreasing of the gain if $(\Delta\gamma_z/\gamma_z) \ll 1/N$, where N is the number of ripple periods of the wiggler, the thermal effect will not change the gain too much This fact suggests that an optimum system may be a short section of a wiggler with high gain

With regard to the beam energy spread there is the possibility of a hot-cathode source or the preparation of a cold beam using appropiate diode geometry

If the SRB - FEL operates with an exponential gain the two-wave gain also becomes large only if the beam is dense, the pump field is strong, and the length of the wiggler is well chosen. The analysis of high, two-wave gain

case must include the beam thermal spread The theory suggests that FEL efficiency could be high and some more experimental work must be done The simulation method applied to the FEL process in 2*D*-and 3*D*-realistic beam geometries could help to understand this complex mechanism of a FEL-operation

REFERENCES

1 a) P Sprangle, J Plasma Phys **11,** 299 (1974)
b) P Sprangle, V L Granatstein, Appl Phys Lett **25,** 377 (1974)
2 W B Colson, Phys Lett **A 64,** 190 (1977)
3 N M Kroll, W A McMullin, Phys Rev **A 17,** 300 (1978)
4 P Sprangle and A T Dobrot, J Appl Phys, **50,** 2652 (1979)
5 P Sprangle C M Tang and W M Manheimer, Phys Rev Lett **43,** 1932 (1979) 1979), Phys Rev **A 21,** 302 (1980)
6 N M. Kroll, P L Morton and M N Rosenbluth, IEEE J Quantum Electr **QE-17,** 1436 (1981)
7 S I Tsunoda and J H Malmberg, Phys Fluids **27,** 2557 (1984)
8 P Sprangle, C M Tang and C W Roberson, Nucl Instr Methods, Phys Res **A 239,** 1 (1985), Appl. Phys Lett **39,** 677 (1981)
9 W B Colson, G Dattoli and F Ciocci, Phys Rev **A 27,** 1399 (1983)
10 W B Colson and R S Freedman, Phys Rev **A 31,** 828 (1985)
11 B Hafizi, A Ting, P Sprangle and C M Tang, Phys Rev **A 38,** 197 (1988), Phys Fluids **31,** 1708 (1988), 3387 (1988)
12 H P Freund, A K Ganguly, Phys Rev **A 28,** 3438 (1983)
13 A K Ganguly and H P Freund, Phys Rev **A 32,** 2775 (1985), Phys Rev **A 34,** 1242 (1986)
14 D B Mc Dermott, T C Marshall, S P Schlesinger and V L Granatstein, Phys Rev Lett **41,** 1368 (1990)
15 P Sprangle and R A Smith, Phys Rev **A 21** 293 (1980)
16 D A G Deacon, L R Elias and J M J Madey, Phys Rev Lett **38,** 892 (1977)
17 R C Davidson, H S Uhm, Bull Amer Phys Soc **24,** 1066 (1979)
18 J R Cary and T J Kwan, Bull Amer Phys Soc, **24,** 1068 (1979)

STUDIA UNIV BABEŞ-BOLYAI, PHYSICA, XXXVI, 1, 1991

THERMISTANCE SEMIREFRACTAIRE EN MICROSERIE DE LABORATOIRE

C. CODREANU*, T. NICOLAU**, S. CODREANU***

Resumé. — Sur deux microséries de laboratoire on a été étudié et etabli le régime thermique du viellissement artificiel qui a conduit à une themistance fiable et stable, avec le coefficient thermique de la résistence d'environ 2%/°C jusqu'à 160 °C

1 *Introduction* Si pour des températures pas trop élevées (100 °C) il existe une grande diversité des thermistances commercialisées, dans le domaine des températures plus elevées, l'offre est beaucoup plus faible. En effet, en ce cas la réalisation d'une haute fiabilité et stabilité des paramétres physiques et fonctionaux des thermistances éxige une technologie de pointe.

Nous avons réalisé une thermistance-perle, protégée en verre, dont la substance active est une céramique $CoO—MnO—Al_2O_3—LaB_6$, cuite à 1 600 °C, en faisceau LASER, suivant une technologie brevetée [1], dont les caractéristiques, thermique $R(T)$ et statique courant-tension $I(U)$, sont présentées sur les figures (1) resp. (2)

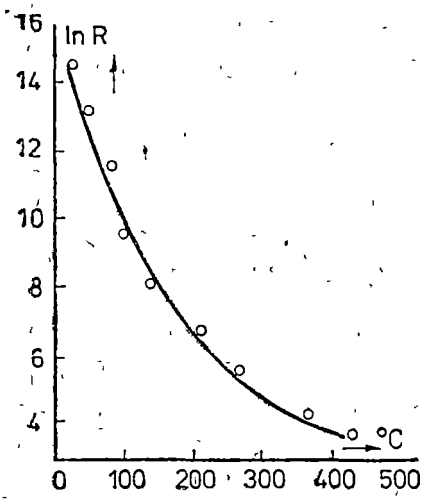

Fig 1 La caractéristique thermique typique ln R = f(T) de la thermistance

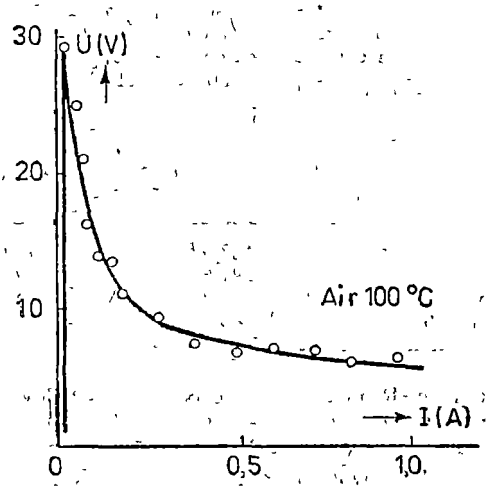

Fig. 2 La caractéristique volt-ampérique statique typique (avec effet— relais) de la thermistance, en air calme à 100 °C

* *Instit Polytechnique Cluj-Napoca*
** *Inst National de Metrologie Bucuresti*
*** *Universitè Babeş-Bolyai, 3400 Cluj-Napoca, Roumanie*

Les principaux paramétres sont résistance nominale $R_{25} = 10^2 - 10^3$ kohm, coéfficient thermique de la resistance $\alpha_\rho = (3,5 - 5,0)\,\%/°C$, énergie d'activation thermique $\Delta E = (1,1-1,6)$ eV, constante électronique $B = (5000-7\,000)$ K, [2]

Le fait le plus important c'est que α_ρ se mentient aux valeurs assez élevées mème pour des températures supérieures à 100°C, ce qui permettrait l'utilisation de ce modèle de thermistance dans ce domaine de température

2 *Expérimnt et discussions* Dans ce but nous avons réalisé deux micro series de 100 thermistances chacune, qui ont été soumises à un régime de viellissement artificiel, en observant l'évolution de la dispersion de la valeur de la résistance nominale, comme critère de la stabilité des paramètres et des propriétés physiques des thermistances

Le traitement thermique de viellissement à été réalisé sous deux variantes, *A* et *B*, à savoir:

— première phase choc thermique à 400°C, 150h (var *A*) et à 330°C, 1000 h (var *B*),

— deuxième phase cycles de rechauffements-refroidissements entre (25—330)°C (var *A*) et entre (25—250)°C (var *B*), la durée de chaque période „chaude" étant de 1000 *h*

Toutes les opérations ont été effectuées dans des conditions métrologiques standar d[1]

Initialement les thermistances ont éte rangées dans des groupes de dix exemplaires, dont les valeurs de R_{25}, après le choc thermique, sont données sur le tabl 1, pour les deux variantes **A** et **B**.

Tabl 1

R_{25}(min) et R_{25}(max)

var		17,7	50,8	148,6	196,7	228,0	243,7	269,5	297,0	334,8	454,8
	A	47,2	139	186,5	222,6	242,0	268,0	295,6	334,0	422,2	1036
var		30,1	65,2	75,8	80,7	85,1	88,7	91,8	97,2	102,8	131,2
	B	63,0	74,6	79,5	84,5	88,7	91,7	97,2	102,8	128,1	165,1

Ainsi comme on observe, la variante *B* conduit a une reduction de la dispersion de R_{25}, de 1018 kohm (var *A*) jusqu'à 135 kohm (var *B*)

Ulteireurement, de chaque groupe nous avons sélectionné 3—4 thermistances, dont la dispersion de la R_{25} est très faible, tabl 2

Tabl 2

R_{25}(min) et R_{25} (max), après le choc

var		38,2	182,9	199,5	212,6	138,2	238,0	268,0	292,8	331,0
	A	38,3	187,5	202,2	212,9	147,7	242,9	272,9	295,5	334,0
var		60,2	65,2	78,8	81,2	86,7	88,7	91,8	98,9	104,4
	B	63,0	66,1	79,1	82,5	87,3	89,5	93,7	100,6	107,9

qui ont été soumises à la deuxième phase du viellissement, en suivant la variation relative $\Delta R/R$ pour chaque thermistance, en fonction de temps Comme titre d'exemple, nous présentons les résultats typiques seulement pour une seule groupe de chaque variante *A*, *B*, sur les Fig 3 resp 4

3 **Conclusions.** En analysant toutes les groupes il en resulte qu'on obtient la stabilisation des propriétés physiques après 4—5 cycles rech -refr-, après quoi on observe une tendence de croissance de la dispersion relative de la résistance nominale

[1] A l'Inst National de Metrologie Buc

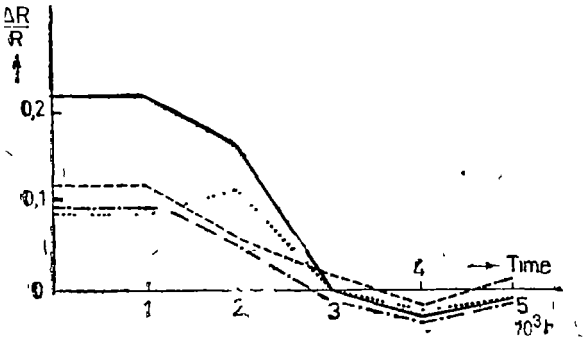

Fig. 3 La variation relative $\Delta R/R$, au cours du viellissement forcé (premier groupe)

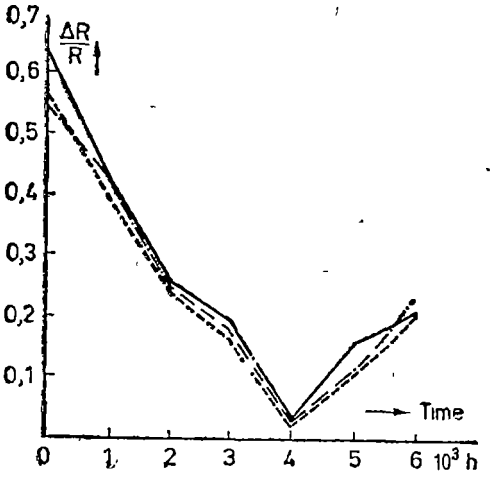

Fig. 4. La variation relative $\Delta R/R$, au cours du viellissement forcé (deuxième groupe)

La dispersion finale de la R_{25} stabilisée, correspondrait à une erreur de (0,5—3)°C, pour la variante **A** et de seulement $\pm 0,1$°C, pour la variante **B** au cas où la thermistance serait utilisée comme thermomètre, ce qui représente une véritable performance

Avec un α_ρ assez grand, une caractéristique statique $U(I)$ avec effet de relais et une très bonne fiabilité et stabilité des paramètres, ce type de thermistance est très recommandable dans des differents schèmas de mésure et controle de température jusqu'à $T_{max} = 160$°C.

REFERENCES

1 C Codreanu, I Cosma, M Vancea, Certif inv 68105/1974
2 C Codreanu, S Codreanu, *Thermistance-perle miniaturisée semirefractaire*, Progr Phys., Buc 1987, pg 199

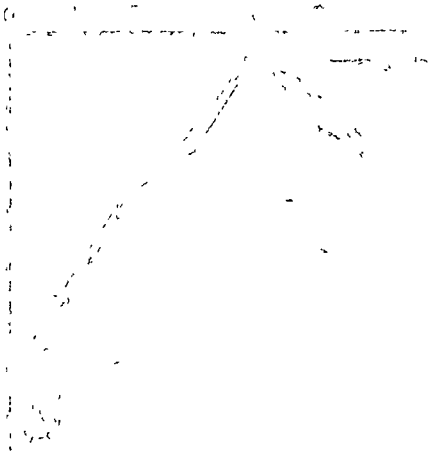

STUDIA UNIV BABEŞ-BOLYAI, PHYSICA, XXXVI, 1, 1991

ULTRASOUND ABSORPTION IN ETHANOL + P-XYLENE SYSTEM

ILEANA LENART*, AURELIA CIUPE*, D. AUSLÄNDER*

ABSTRACT. The nature and intensity of intermolecular interactions in mixtures formed of a polar component — ethanol — and a non polar one — *p*-xylene — were studied by the ultrasonic method The data on the propagation velocity of the ultrasound and the density, previously presented, as well as the results of the measurement of ultrasound absorption and of dynamical viscosity have permitted to calculate the relaxation absorption, the volumic viscosity and the viscosity relaxation times The ultrasonic perturbations of the molecular equilibrium cause structural and thermal relaxation absorption, and also the desactivation of the molecules, being in excited state of vibration The variation of these magnitudes with the increase of ethanol concentration in mixtures, was correlated with the modifications of the interactions between the molecules of the components

1. **Introduction.** The study of the molecular-acoustic properties of the ethanol + p-xylene system was dealt with in a previous work [1] by determining the concentration dependence of the ultrasound propagation velocity, adiabatic compressibility and of the free intermolecular distance and available volume, respectively

Following the researches [2], [3] on the system formed of a polar component, with associated molecules, and of a nonpolar one, we aim at correlating the intermolecular interactions with the relaxation processes by ultrasound absorption measurements.

2. **Theory.** According to the viscoelastic theory, by admitting the additivity of attenuation constants and neglecting the non-significant ones in fluids, the ultrasound absorption is expressed by

$$\frac{\alpha_{v\,e}}{f^2} = \frac{2\pi^2}{\rho c^3}\left(\frac{4}{3}\eta + \eta_V\right) \tag{1}$$

where $\alpha_{v\,e}$ is the attenuation constant by absorption of the viscoelastic theory, f and c the frequency and the ultrasound propagation velocity, ρ the density, η and η_V the dynamical viscosity and the volumic viscosity of the liquid, respectively.

The calculable term

$$\frac{\alpha_{vis}}{f^2} = \frac{8}{3}\frac{\pi^2}{\rho c^3}\eta \tag{2}$$

represents the viscosity absorption, and the term

$$\frac{\alpha_V}{f^2} = \frac{2\pi^2}{\rho c^3}\eta_V \tag{3}$$

* University Babeş-Bolyai, Department of Physics, 3400 Cluj-Napoca, Romania

which is not calculable due to the volumic viscosity, represents the contribution to the absorption of the relaxation processes correlated with the properties of the compressibility modulum If one admits that the totality of relaxation processes is described in terms of viscosity relaxation, we shall have

$$\frac{\alpha_{v\,e}}{f^2} = \frac{\alpha_{exp}}{f^2} \tag{4}$$

and thus, from the relation (1) it results

$$\eta_V = \frac{\rho c^3}{2\pi^2}\left(\frac{\alpha_{exp}}{f^2} - \frac{\alpha_{vis}}{f^2}\right) \tag{5}$$

By correlating the relaxation mechanisms with the properties of the compressibility modulum the relaxation time is obtained:

$$\tau_V = \beta_S(2\eta + \eta_V) \tag{6}$$

β_S being the adiabatic compressibility coefficient

3. **Experimental.** All the measurements were carried out in the components of the system as well as in a series of concentrations, under constant temperature conditions, at $20° \pm 0{,}05°C$ temperature. The dynamical viscosity was measured by means of a Höppler viscosimeter, and the attenuation constant of ultrasouns — by the impulse method on the basis of the repeated echoes at a fixed distance, at 8 MHz frequency.

4 **Results.** By using the experimental data of the previous measurements of the density and of the ultrasonic velocity, together with the above mentioned ones, we calculated the values of viscosity absorption at different ethanol concentrations on the basis of the formula (2):

Fig. 1 shows the absorption variation obtained by calculation, and the variation of experimental absorption with the increase of alcohol concentration.

The viscosity absorption increases from p-xylene to alcohol along a curve, the slope of which progressively increases, especially in the field of high alcohol concentrations.

The experimental absorption, having much higher values than in the case of the calculated one, is characterized by a pronounced maximum at $\chi_{et} = 0.1$.

The relaxation absorption expressed by the relation (3), calculated from: $\frac{\alpha_{rel}}{f^2} = \frac{\alpha_{exp}}{f^2} - \frac{\alpha_{vis}}{f^2}$ is presented in Table I One can observe the value of the relaxation absorption in p-xylene, which is about twice higher than that corresponding to the ethanol.

The specific relaxation absorption of ethanol:

$$\frac{1}{\chi_{et}} \cdot \frac{\Delta\alpha_{rel}}{f^2}, \text{ where } \Delta\alpha_{rel} = \alpha_{rel\,(syst)} - \alpha_{rel(p\text{-xylene})}$$

varies with the concentration along the curve of Fig. 2.
Since at concentrations superior to the fraction $\chi_{et} = 0.54$, $\alpha_{rel(syst)} < \alpha_{rel(p\text{-xylene})}$, in this range the specific relaxation absorption will have negative values.

The values of some absorption parameters are shown in Table I

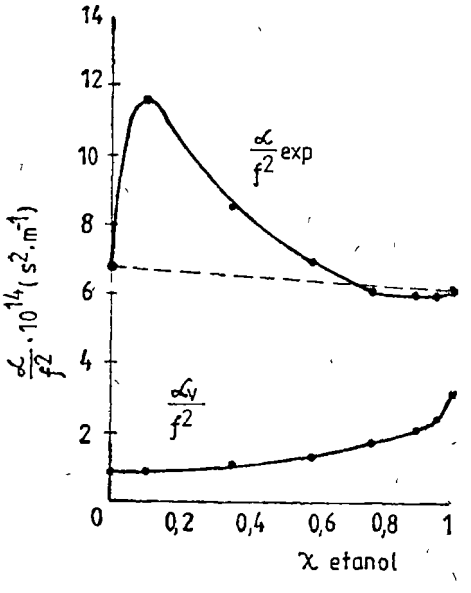

Fig 1 The variation of the absorption $\left(\frac{\alpha}{f^2}\right)$ against the mole fraction of alcohol

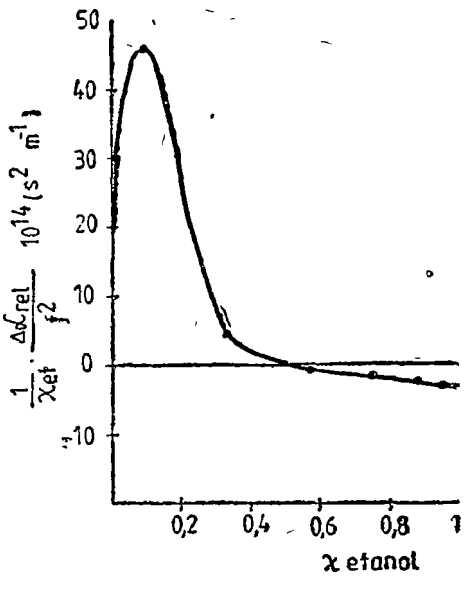

Fig 2 The variation of specific absorption of ethanol $\left(\frac{1}{\chi_{et}} \cdot \frac{\Delta\alpha_{rel}}{f^2}\right)$ against the mole fraction of alcohol.

Table I

Conc $\chi_{ethanol}$	$\frac{\alpha_{exp}}{\alpha_{visca_n}}$	$\eta \ 10^3$ (Ns/m^2)	$\eta_V \ 10^3$ (Ns/m^2)	$\frac{\eta_V}{\eta}$	$\frac{\alpha_{rel}}{f^2} \cdot 10^{14}$ (s^2m^{-1})
0	8,73	0,659	6,09	9,241	5,94
0,100	13,81	0,661	10,22	15,460	10,51
0,345	8,52	0,733	6,79	9,270	7,44
0,585	5,56	0,850	4,81	5,661	5,61
0,760	3,98	1,013	3,58	3,538	4,41
0,894	3,15	1,205	3,01	2,497	3,93
0,950	2,70	1,318	2,57	1,950	3,47
1,000	2,14	1,492	1,96	1,317	3,07

The curve of Fig 3 illustrates the variation of the relaxation time with the ethanol concentration, the values being calculated from the relation (6). After an increase up to a maximum placed at about $\chi_{et} = 0\,3$, the relaxation time linearly decreases till $\chi_{et} = 0\,6$, at higher concentrations displaying a tendency toward a concentration independence.

5 **Discussions.** The relaxation absorptions result from the mechanisms of energetical exchanges accompanying the re-equilibrating of the system perturbed by the wave through periodical variations of pressure and temperature.

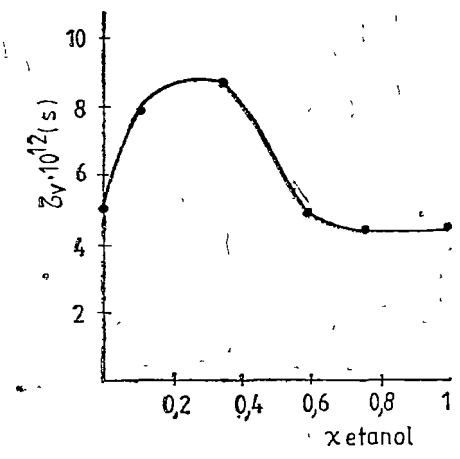

Fig 3 The variation of relaxation time against the mole fraction of alcohol

The equilibria are determined by the intermolecular interactions corresponding to the properties of the molecules of the propagation medium

The components of the studied system are characterized by different molecular structures the p-xylene molecules, with zero dipole-moment are characterized by a molecular mass and sizes superior to that of the other component, having a plane configuration, they form relatively compact arrangements Van der Waals dispersion forces are acting between these molecules at the level of methyl radicals. Taking into account their polar character, besides interactions of the hydrocarbonate radicals by Van der Waals forces, the ethanol molecules form by means of hydrogen bounds, dimer, respectively trimer associations [4], [5], [6].

In the mixture, all the intermolecular forces, which are specific to the components, undergo modifications due to the interactions between the molecules of different species After the disappearance of hydrogen bounds between the alcohol molecules and of the interaction of p-xylene molecules by dispersion forces, the dispersion and induction forces between p-xylene and ethanol molecules are settled, together with the increase of ethanol concentration, owing to the strong polarizability of the benzene ring, by the continuing increase of ethanol concentration, the hydrogen bounds are re-established, forming alcohol molecular associations

The ultrasonic perturbations of molecular equilibria, accompanied by volume and entalpy variations bringing about the structural and thermic relaxation absorption, are correlated with the compressibility of the system, formed of the sum of a structural term and of a vibrational one

The studied system is characterized by three principal mechanisms of relaxation absorption 1 The structural absorption resulting from the perturbation of molecular association $\rightleftarrows$ disassociation equilibria, 2 Thermic relaxation caused by the energy exchanges between the external and internal degrees of freedom; 3 The disactivating of the molecules being in an excited vibration state by non-elastic collisions between the molecules of the components, this mechanism contributes to the decrease of absorption

The first process, characteristic to ethanol, is the result of the phase difference of energy exchanges between the system and the wave, imposed by the ultrasound frequency

In the very diluted mixtures, the pronounced diminution of the interactions contributes to the favouring of the mechanism 2, manifested by the pronounced increase of relaxation absorption The increase of alcohol concentration limits the intensity of thermic relaxation through the setting of polar-nonpolar interactions, simultaneously with the setting of the effect 3 Finally, the con-

tinuous increase of alcohol concentration has as result the prevalence of the mechanism 1

The relaxation time calculated from the formula (6) renders a general value of the times corresponding to all relaxation processes

For a single relaxation process

$$\frac{\alpha_{rel}}{f^2} = \frac{A}{1 + \left(\frac{f}{f_0}\right)^2}$$

where A is the relaxation amplitude, and f and f_0 are the ultrasound frequency, and the relaxation frequency respectively, for the given experimental conditions. $\frac{f}{f_0} \to 0$, therefore $\frac{\alpha_{rel}}{f^2} \to A$

Taking into consideration all the relaxation processes:

$$\frac{\alpha_{rel}}{f^2} = \sum_{i=1}^{i=n} \frac{A_i}{1 + \left(\frac{f}{f_0}\right)^2}$$

one can obtain the corresponding times, having values superior to that resulting from the relation (6)

REFERENCES

1 Ciupe A, Lenart I, Auslander D — Academia R S România, Sesiunea de Comunicări de Acustică, București, 13—14 oct 1989
2 Lenart I, Auslander D, Ciupe A — Studia Universitatis Babeș-Bolyai, Physica, **XXXIV**, 1989, 2, p 42—45
3. Lenart I, Ciupe A, Auslander D — Studia Universitatis Babeș-Bolyai, Physica **XXXIII**, 1988, 2, p 20—25
4 Nigam, R K, Singh, P P — Trans Faraday Soc **65**, 1969, 950
5 Lang J, Zana R — Trans Faraday Soc 567, vol **66**, Part 3, March, 1970, p. 597—604
6 Prakash O, Srivastava A, Darbari S — Acustica, vol **72** (1990) p 292—294.

STUDIA UNIV BABEŞ-BOLYAI, PHYSICA, XXXVI, 1, 1991

THE ULTRASONIC STUDY OF N-PROPILIC ALCOHOL + O-XYLENE AND N-BUTYLIC ALCOHOL + O-XYLENE SYSTEMS

AURELIA CIUPE,* ILEANA LENART*, D. AUSLÄNDER,* L. MIRCEA*

ABSTRACT. — Ultrasonic velocity and attenuation constant by absorption, dynamic viscosity and density measurements have been carried out in n-propanol + ortoxylene and n-butanol + ortoxylene mixtures The results concerning the calculated values for the adiabatic compressibility, the internal pressure, the disponible volume, the volumic viscosity, the classical and the structural absorption, the relaxation frequency as well as that of some excess quantities give structural information about the studied mixtures

The experimental results allowed the evaluation of intermolecular interactions and their change with concentration in function of the polar configuration of components' molecule and the length of carbonic chain

Theoretical considerations. The previous research [1], [2], [3], [4] of a series of binary mixtures of organic liquids emphasized the reflection of structural properties at molecular level by means of ultrasonic propagation constants. The present study shows the results of the research carried out in n-propanol + o-xylene respectively n-butanol + o-yxlene mixtures

The ultrasonic velocity and adiabatic compressibility being defined by:

$$c_s^2 = \left(\frac{\partial p}{\partial \rho}\right)_s \tag{1}$$

$$\beta_s = -\frac{1}{V}\left(\frac{\partial V}{\partial p}\right)_s \tag{2}$$

results

$$\beta_s = \frac{1}{\rho c^2} \tag{3}$$

ρ, p and V being the density, the pressure and the volume.

From the Van der Waals internal pressure

$$p_i = \frac{a}{V^2} = \frac{a}{M^2}\rho^2 = a_y \cdot \rho^2 \tag{4}$$

where $a_y = a/M^2$ factor [5] characterizes the measure of attractive forces between molecules included in $1/M$ fraction of mass unity, M being the molar weight

From the relation (1).

$$c^2 = -\chi \frac{V^2}{M}\left(\frac{\partial p}{\partial V}\right)_T$$

* *University Babeş-Bolyai, Department of Physics, 3400 Cluj-Napoca, Romania*

by making some simplifying operations for a limited temprature range we obtain:

$$p_i = \frac{\rho c^2}{2\chi} \tag{5}$$

χ being the ratio of molar heats at constant pressure and constant volume respectively.

From (4) and (5) results.

$$a_y = \frac{c^2}{2\chi\rho} \tag{6}$$

The disponible volume is calculated based on the relation [6]

$$V_d = V\left(1 - \frac{c}{c_\infty}\right) \tag{7}$$

where. $c_\infty = 1600\ m/s$ represents the ultrasonic limit velocity in an omologue series of organic liquids for $M \to \infty$.

The ultrasonic absorption in liquids is given by the expression:

$$\frac{\alpha}{f^2} = \frac{2\pi^2}{\rho c^3}\left(\frac{4}{3}\eta + \eta_V\right) \tag{8}$$

where: α is the attenuation constant, f — the ultrasonic frequency, η — the dynamic viscosity and η_V — the volumic viscosity.

The two terms in (8) represent the classical absorption, respectively the relaxational one

$$\frac{\alpha_{exp}}{f^2} = \frac{\alpha_{visc}}{f^2} + \frac{\alpha_{rel}}{f^2} \tag{9}$$

which permits the calculation of volumic viscosity:

$$\eta_V = \frac{\rho c^3}{2\pi^2}\left(\frac{\alpha_{exp}}{f^2} - \frac{\alpha_{visc}}{f^2}\right) \tag{10}$$

The relaxation frequency is given by:

$$f_V = \frac{1}{2\pi\beta_s(2\eta + \eta_V)} \tag{11}$$

Experimental. Determinations were carried out at constant and controlled temperature of $20 \pm 0{,}05\,°C$

For the density and dynamic viscosity measurements in mixtures and in the pure compounds capillary picnometer respectively Hoppler viscosymeter were used

Ultrasonic velocity was measured by the optical method of diffraction at $f = 4\ MHz$ frequency.

For measuring attenuation constant through absorption the method of repeated echos at fixed path of 8 MHz impulses was used.

Results. The values of ultrasonic velocity in the two studied systems are included in Table 1.

Using the data in Table I and the values of experimentally determined densities, based on formula (3) it was calculated the concentration dependence of adiabatic compressibility, presented in Fig. 1

Table 1

n-propanol + o-xylene		n-butanol + o-xylene	
χ_{alc}	c $(m\ s^{-1})$	χ_{alc}	c $(m \cdot s^{-1})$
0	1361,5	0	1361,5
0,079	1344,4	0,065	1338,6
0,288	1321,4	0,25	1318,9
0,519	1259,9	0,470	1304,5
0,708	1277,3	0,666	1297,5
0,866	1260,8	0,842	1285,8
0,935	1251,7	0,923	1283,1
1	1257,0	1	1279,4

and the variation of the disponible volume (7) with concentration, presented in Fig 2

The a_y factor, calculated from experimental data by means of formula (6) varies with concentration along the curves from Fig. 3

From velocity, density and viscosity data, classical absorption was calculated, and from the results of absorption measurements, based on expressions (9) and (10) relaxational absorption respectively volumic viscosity were obtained the results being presented in Figs 4 and 5, respectively in Table 2.

Viscosity relaxation frequency, calculated from formula (11) varies with alcohol concentration, in the system along the curves from Fig 6

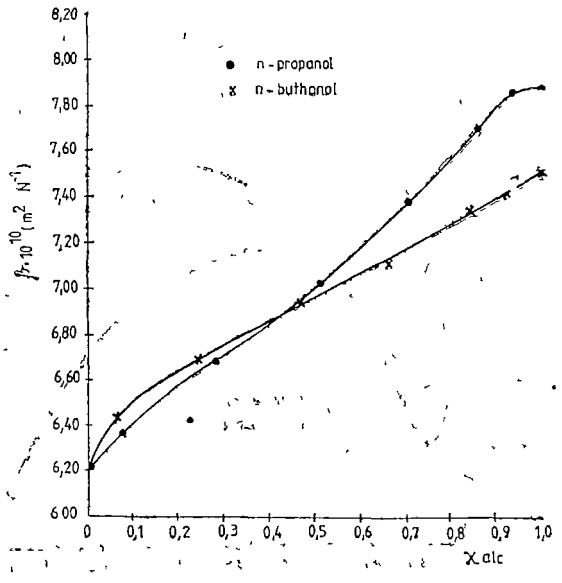

Fig 1 Variation of adiabatic compressibility (β_s) against mole fraction of alcohol (χ_{alc}) in n-propanol + o-xylene and n-butanol + o-xylene mixtures

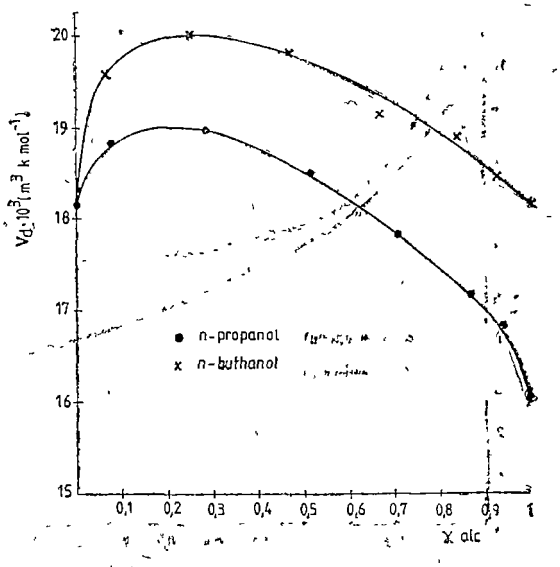

Fig. 2 Variation of disponible volume (V_d) against mole fraction of alcohol (χ_{alc}) in n-propanol + o-xylene and n-butanol + o-xylene mixtures

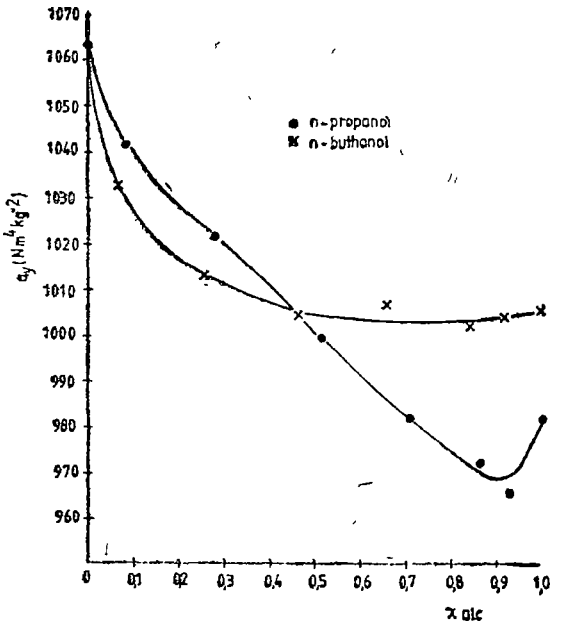

Fig. 3 Variation of a_y factor against mole fraction of alcohol (χ_{alc}) in n-propanol + o-xylene and n-butanol + o-xylene mixtures

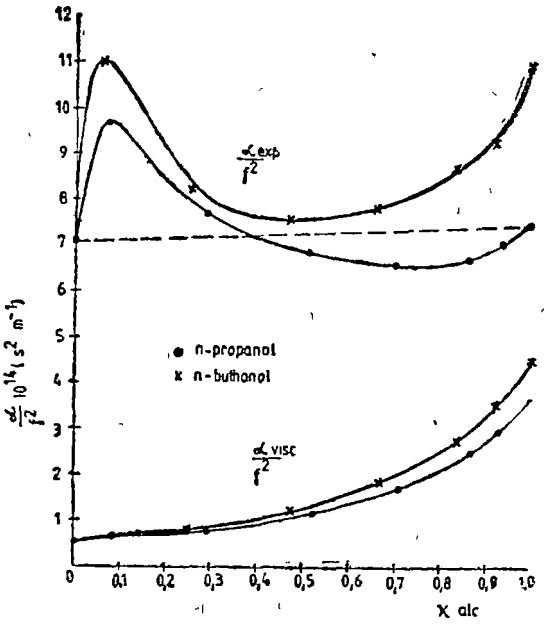

Fig 4 Variation of α_{exp}/f^2 and α_{visc}/f^2 against mole fraction of alcohol (χ_{alc}) in n-propanol+o-xylene and n-butanol + o-xylene mixtures

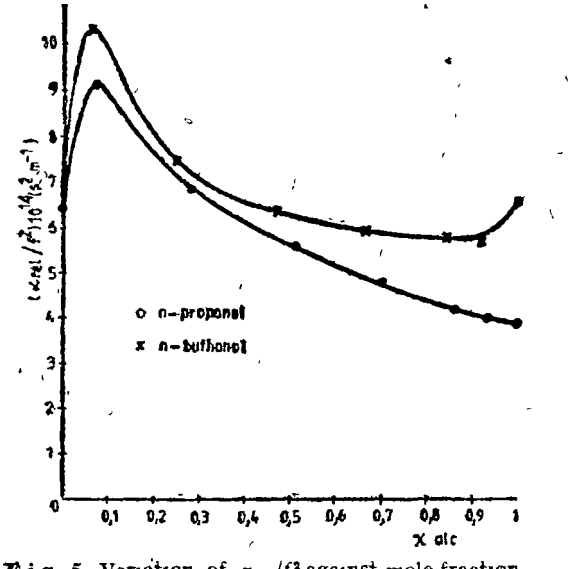

Fig 5 Variation of α_{rel}/f^2 against mole fraction of alcohol (χ_{alc}) in n-propano + o-xylene and n-butanol + o-xylene mixtures.

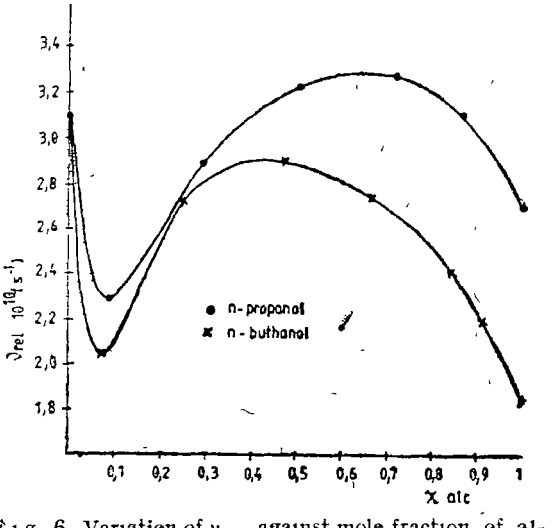

Fig 6. Variation of ν_{rel} against mole fraction of alcohol (χ_{alc}) in n-propanol + o-xylene and n-butanol + o-xylene mixtures

Table 2

n-propanol + o-xylene		n-butanol + o-xylene	
conc (χ_{alc})	$\eta_V \cdot 10^3$ ($N\ s \cdot m^{-2}$)	conc (χ_{alc})	$\eta_V \cdot 10^3$ ($N\ s\ m^{-2}$)
0,0	7,14	0,0	7,04
0,079	9,76	0,065	10,93
0,288	6,82	0,249	7,29
0,519	5,30	0,470	6,08
0,708	4,30	0,666	5,53
0,866	3,49	0,842	5,23
0,935	3,24	0,923	5,01
1,0	3,11	1,0	5,72

Discussion. The investigated systems are formed from components with different molecular structures: o-xylene molecules, having a dipole moment different from zero, interact by Van der Waals forces at metyl radical level, they are characterized by plane configurations, what confer them a compact arrangement

Alcohol molecules form dimer and trimer associations by means of hydrogen bonds, with a higher occurence frequency in propanol Between hidrocarbonate radicals of alcohols Van der Waals forces also act, their intensity increasing with the number of carbon atoms in molecule

These equilibria undergo changes in o-xylene + alcohol systems owing to the interactions between the component molecules Thus, the establishment of some Van der Waals forces between the component molecules have the effect of breaking of hydrogen bonds between the alcohol molecules. This mecanism is favourized in the case of o-xylene + n-butanol system owing to the higher intensities of Van der Waals forces between the CH_3 groups as well as to the lower degree of association by hydrogen bonds

In the range of low concentrations, the screening of alcohol molecules by those of o-xylene hinder the remaking of hydrogen bonds, concomitently, with the diminution of Van der Waals forces between o-xylene molecules, the configuration moves towards a less compact structure This process continues, at concentration increase, with the tendency of eliminating o-xylene — o-xylene interactions and of progressive settling of hydrogen bonds between alcohol molecules

The dependence of ultrasonic magnitudes on intermolecular interactions is generally, neither direct nor exclusive, the specific caracteristics originating from their base as well as from some eventual concessions concerning the rigour, become manifest through the reflection of some different aspects of the equilibrium of the intermolecular forces, respectively of their secondary effects.

Thus, a direct dependence characterizes ultrasonic velocity, adiabatic compressibility and „a_y" factor Structural consequences of the interactions are given by the disponible volume, the dynamic viscosity and the viscosity absorp-

tion Complex secondary mechanisms, having an energetic character, are reflected by the relaxational absorption, the volumic viscosity and the relaxation frequency

The ultrasonic velocity and the compressibility of systems, functions of media elasticity, depend on the intermolecular forces, as well as on the space configuration of molecules The variation of compressibility with alcohol concentration and the differenciation of these values in the two systems corresponds to the specified evolution of interactions.

The maximum of compressibility at high concentration of propanol probably comes from

a) the disappearence of xylene — xylene Van der Waals forces,

b) the restriction of n-propanol molecular associations by alcohol — xylene Van der Waals forces,

c) a looser molecular configuration

The „a_v" factor represents a measure of attractive forces in a Van der Waals liquid, the calculation of the expression imposing some approximations. Its variation with concentration relieves the presence, at low concentrations, of orto-xylene — alcohol Van der Waals interactions and of those of o-xylene — o-xylene interactions in excess, and at high concentrations, o-xylene — alcohol Van der Waals interactions and molecular associations of alcohol in excess.

A minimum value of the attractive forces is situated approximately at the concentration corresponding to the maximum compressibility in the o-xylene + n-propanol system

The disponible volume results from the use of limit velocity of constant value, obtained by the extrapolation made, based on an empirical model. Its variation with the concentration reflects as compressibility does, the evolution of the system, under the influence of interaction change, towards a loose structure An analogue process is illustrated by the negative deviation from linearty of dynamic viscosity owing to the increase of the free volume in the mixtures

The differentiation of a_y, V_d and η behaviour in connection with the nature of alcohol corresponds to the differences concerning the interaction intensity of respective molecules

The connexion between ultrasonic absorption and intermolecular interactions permitted the classification of liquids based on the value of $\alpha_{exp}/\alpha_{visc}$ ratio. According to this criterion, o-xylene belongs to the group of liquids with weak interactions, for which $3 < \alpha_{exp}/\alpha_{visc} < 400$, and the alcohols belong to the group of those with stronger interactions for which $1 < \alpha_{exp}/\alpha_{visc} < 3$

The variation of the absorption ratio with concentration shows an increase until a maximum at $\chi_{olc} = 0{,}08$, followed by a diminution until its value in alcohol. Therefore, the systems belong to the group of liquids with weak interactions till the concentration $\chi_{alc} = 0{,}8$ after which they have a behaviour characterized by strong interactions If the change of α_{visc} with concentration is determined by the dynamic viscosity change, the contribution of the structural component of absorption results from the wave energy transmission processes to the external and internal degrees of freedom followed by relaxational phenomena characterised through different frequencies.

Besides these, at higher alcohol concentration, association-dissociation relaxational processes of molecular grouping can occur, they being disturbed by the propagation of ultrasonic wave in the medium

The intermolecular collisions in the case of extreme concentration ranges between the two compounds can also affect the intensity of energetic exchanges between the degrees of freedom, thus contributing to the change of relaxation frequencies, respectively of the ultrasonic absorption values

REFERENCES

1 Lenart I, Ciupe A, Auslander D, Lender E — Academia Română, Comisia de Acustică Sesiunea de Comunicări, București, Oct 1987 — oct 1988, Caietul **23**, p 73—76.
2 Lang, I, Zana R —Trans of Faraday Soc 567, vol **66**, Part 3 March 1970, p 597—604.
3 Srinivasa Rao P, Subha N C S, Narayana Swamy — Acustica, vol **75** (1991), p 86—89.
4 Lenart I, Auslander D., Ciupe A — Studia Univ Babeș-Bolyai, Physica, **XXXIV**, 2, 1989, p 42—45
5. Melkonean — *Primenenie ul'trazvuk k essledovanie vescestvo* MOPI, Moskva 1956
6. Schaafs W, — *Molekularakustik*, Springer Verlag, Berlin, 1963

STUDIA UNIV. BABEŞ-BOLYAI, PHYSICA, XXXVI, 1, 1991

THERMOSOLUTAL INSTABILITY OF A COMPOSITE ROTATING PLASMA IN THE PRESENCE OF THE SUSPENDED PARTICLES

MIRCEA VASIU*

ABSTRACT. The influence of the suspended particles on the onset of Benard convection is studied in the presence of a vertical magnetic field and of a uniform rotational motion The effect of finite Larmor radius (FLR effect) of a composite plasma in the presence of the uniform solute gradient is also studied.

Introduction In this paper we have generalized the results obtained in [1]–[4]. The plasma consists of a ionized component and a neutral component. The ionized component is incompressible, viscous, with finite resistivity (finite magnetic viscosity), in uniform rotational motion with angular velocity $\vec{\Omega}(0, 0, \Omega)$. Also it is under the influence of a uniform vertical magnetic field $\vec{B}(0, 0, B_0)$ and at the same time under the influence of the gravitational acceleration $\vec{g}(0, 0, -g)$ The neutral component is assumed to be incompressible and viscous. Consider an infinite horizontal plasma layer of thickness d heated from below and subjected to a uniform gradient temperature and a uniform solute gradient. In the present study we have investigated the role of viscosity for the plasma and at the same time the collision interaction between the charged particles(ions) and neutral particles

Perturbation Equations Taking a small perturbation of the steady-state, we get the linearized *MHD* equations in the form

$$\frac{\partial \vec{u}}{\partial t} = -\frac{1}{\rho_0}(\nabla \delta p + \nabla \delta \vec{p}) + \nu \Delta \vec{u} + \delta(\vec{v} - \vec{u}) + \varepsilon \nu_c (\vec{u}_n - \vec{u}) + (\alpha' \gamma - \alpha \theta)\vec{g} + 2\vec{u} \times \vec{\Omega} + \frac{1}{\mu_0 \rho_0}(\nabla \times \delta \vec{B}) \times \vec{B} \tag{1}$$

$$\frac{\partial \vec{u}_n}{\partial t} = -\nu_c (\vec{u}_n - \vec{u}) + \nu_n \Delta \vec{u}_n \tag{2}$$

$$\left(\tau \frac{\partial}{\partial t} + 1\right)\vec{v} = \vec{u} \tag{3}$$

$$\nabla \vec{u} = 0, \quad \nabla \cdot \vec{u}_n = 0 \tag{4}$$

$$\frac{\partial}{\partial t}(\delta \vec{B}) = \nabla \times (\vec{u} \times \vec{B}) + \nu_m \Delta \delta \vec{B} \tag{5}$$

$$\left(\frac{\partial}{\partial t} - \varkappa \Delta\right)\theta = \beta u_z \tag{6}$$

$$\left(\frac{\partial}{\partial t} - \varkappa' \Delta\right)\gamma = \beta' u_z, \tag{7}$$

* *University Babeş-Bolyai, Department of Physics, 3400 Cluj-Napoca, Romania*

where $\vec{u}(u_x, u_y, u_z)$, $\vec{u}_n(u_{nx}, u_{ny}, u_{nz})$, $\delta\vec{B}(\delta B_x, \delta B_y, \delta B_z)$, $\vec{v}(v_x, v_y, v_z)$, δp, $\delta\overleftrightarrow{P}$, θ, γ denote perturbations in velocity of the ionized component, velocity of the neutral componet, magnetic field, velocity of the suspended particles, pressure of the plasma, stress tensor, density of the ionized component, temperature and concentration, respectively, $\Delta = \nabla^2$

The change $\delta\rho$ in density caused by the perturbations θ and γ is given by

$$\delta\rho = -\rho(\alpha\theta - \alpha'\gamma) \tag{8}$$

The quantities β, β', α, α', $\varkappa$, $\varkappa'$, denote, respectively, the temperature gradient, the solute gradient, the thermal coefficient of expansion, solvent coefficient thermal diffusivity and solute diffusivity.

For the vertical magnetic field, the perturbations $\delta\overleftrightarrow{P}$, for the stress tensor $\overleftrightarrow{P}$ have the components

$$\delta P_{xx} = -\nu_0\rho\left(\frac{\partial u_x}{\partial y} + \frac{\partial u_y}{\partial x}\right),\ \delta P_{yy} = \nu_0\rho\left(\frac{\partial u_x}{\partial y} + \frac{\partial u_y}{\partial x}\right),$$

$$\delta P_{zz} = 0,\ \delta P_{xy} = \delta P_{yx} = \nu_0\rho\left(\frac{\partial u_x}{\partial x} - \frac{\partial u_y}{\partial y}\right), \tag{9}$$

$$\delta P_{yz} = \delta P_{zy} = 2\nu_0\rho\left(\frac{\partial u_z}{\partial x} + \frac{\partial u_x}{\partial z}\right),\ \delta P_{xz} = \delta P_{zx} = -2\nu_0\rho\left(\frac{\partial u_y}{\partial z} + \frac{\partial u_z}{\partial y}\right)$$

The perturbations have the form

$$\delta\varphi(x, y, z, t) = \varphi^x(z)\exp\,](ik_x x + ik_y y + nt), \tag{10}$$

where $\varphi^x(z)$ is the amplitude, k_x, k_y are the wave number along x and y directions and n is the growth rate. Using (10) and an adequate mathematical method [2], the equations (1)—(7) can be brought to the form

$$(D^2 - a^2 - p_1\sigma)\,\Theta = -\left(\frac{\beta d^2}{\varkappa}\right)W \tag{11}$$

$$(D^2 - a^2 - p_3\sigma)\Gamma = -\left(\frac{\beta' d^2}{\varkappa'}\right)W \tag{12}$$

$$(D^2 - a^2 - \sigma_\delta)Z = -\left(\frac{\nu_0}{\nu d}\right)(2D^2 + a^2)\,DW - \left(\frac{B_0 d}{\mu_0\rho\nu}\right)DX - \left(\frac{2\Omega d}{\nu}\right)DW \tag{13}$$

$$(D^2 - a^2 - p_2\delta)K = -\left(\frac{B_0 d}{\nu_m}\right)DW \tag{14}$$

$$(D^2 - a^2 - \sigma_\delta)(D^2 - a^2)W = \left(\frac{\nu_0 d}{\nu}\right)(2D^2 + a^2)DZ + \left(\frac{\alpha g d^2}{\nu}\right)a^2\Theta - \left(\frac{\alpha' g d^2}{\nu}\right)a^2\Gamma -$$

$$-\left(\frac{B_0 d}{\mu_0\rho\nu}\right)(D^2 - a^2)DK + \left(\frac{2\Omega d^3}{\nu}\right)DZ \tag{15}$$

$$(D^2 - a^2 - p_2\sigma)X = -\left(\frac{B_0 d}{\nu_m}\right)DZ, \tag{16}$$

where ν_0 is the gyroviscosity ($\nu_0 = \text{const}/\omega_i$, ω_i is the ion gyration frequency), ν_m is the electrical resistivity of the ionized component, ν is the kinematic viscosity, ρ_0 is the density of the ionized component, $D^2 = d^2/dz^2$, $k^2 = k_x^2 + k_y^2$, $\zeta = (\nabla X \vec{u})_z$, $\xi = (\nabla X \delta\vec{B})$, $W(z)$, $\Theta(z)$, $\Gamma(z)$, $Z(z)$, $X(z)$, $K(z)$ are the amplitudes of the perturbations u_z, θ, γ, ζ, ξ, δB_z respectively, σ_δ have the form: $\sigma_\delta = n_\delta d^2/\nu$, where

$$n_\delta = n\left(1 + \frac{\nu_c \varepsilon}{n\nu_c + \nu_n k^2}\right) + \frac{\tilde{\delta} n\tau}{n\tau + 1} + \frac{\varepsilon \nu_c \nu_n k^2}{n + \nu_c + \nu_n k^2}, \tag{17}$$

where $\varepsilon = \rho_n/\rho$, ρ_n is the density of the neutral component, ν_c is the ion-neutral collisional frequency, $\tilde{\delta} = \varepsilon_p/\tau$, $\varepsilon_p = \rho_p/\rho$ is the mass concentration of the suspended particles (ρ_p is the mass density of the suspended particles, τ is the relaxation time). Introducing the quantities

$$c_1 = \frac{\beta d^2}{\varkappa},\ c_2 = \frac{\beta' d^2}{\varkappa'},\ c_3 = \frac{B_0 d}{\mu_0 \rho \nu},\ c_4 = \frac{\nu_0}{\nu d},\ c_5 = \frac{B_0 d}{\nu_m},\ c_6 = \left(\frac{\alpha g d^2}{\nu}\right) a^2,$$

$$c_7 = \left(\frac{\alpha' g d^2}{\nu}\right) a^2,\ c_8 = \frac{\nu_0 d}{\nu},\ c_9 = \frac{B_0}{\nu_m d},\ c_{10} = \sqrt{T}/d,\ c_{11} = \sqrt{T} d,\ U = \frac{\nu_0^2}{\nu^2},$$

$$\sigma = nd^2/\nu,\ V = 2\Omega d^2/\nu_0,\ p_1 = \nu/\varkappa,\ p_2 = \nu/\nu_m,\ p_3 = \nu/\varkappa',\ \sigma_\delta = n_\delta d^2/\nu, \tag{18}$$

where $a^2 = k^2 d^2$ and the operators

$$O = D^2 - a^2,\ O_\delta = D^2 - a^2 - \sigma_\delta,\ O_1 = D^2 - a^2 - p_1\sigma,\ O_2 = D^2 - a^2 - p_2\sigma$$
$$O_3 = D^2 - a^2 - p_3\sigma,\ O_a = 2D^2 + a^2, \tag{19}$$

the equations (11)—(16) can be reduced to the form

$$O_1(\Theta) = -c_1 W \tag{20}$$

$$O_3\Gamma = -c_2 W \tag{21}$$

$$O_\delta Z = -c_4 O_a DW - c_3 DX - c_{11} DW \tag{22}$$

$$O_2 K = -c_5 DW \tag{23}$$

$$O_\delta OW = c_8 O_a DZ + c_6\Theta - c_7\Gamma - c_9 ODK + c_{11} DZ \tag{24}$$

$$O_2 X = -c_5 DZ \tag{25}$$

Dispersion Equation. Using a proper mathematical method [5] we obtain the dispersion equation. By eliminating the functions Θ, Z, K, Γ, X from equations (20)—(25) we obtain the following equation

$$[(D^2 - a^2 - p_2\sigma)(D^2 - a^2 - \sigma_\delta) - QD^2]\{[(D^2 - a^2 - p_1\sigma)(D^2 - a^2 - p_3\sigma)(D^2 - a^2)][(D^2 - a^2 - p_2\sigma)(D^2 - a^2 - \sigma_\delta) - QD^2] + (D^2 - a^2 - p_2\sigma)a^2[R(D^2 - a^2 - p_3\sigma) - S(D^2 - a^2 - p_1\sigma)]\}W =$$
$$= -U[V + (2D^2 + a^2)]^2(D^2 - a^2 - p_2\sigma)^2(D^2 - a^2 - p_1\sigma)(D^2 - a^2 - p_3\sigma)D^2 W, \tag{26}$$

where $Q = B_0^2 d^2/\mu_0 \rho \nu \nu_m$ is the Chandrasekhar number, $R = \alpha\beta g d^4/\varkappa\nu$ is the thermal Rayleigh number, $S = \alpha'\beta' g d^4/\varkappa'\nu$ is the solute Rayleigh number.
The equation (26) generaliszes the dispersion equation obtained by Gupta and Singh [4], Vasiu [3], [2]

For *stationary convection* ($n = 0$, $\sigma = 0$, $n_\delta = 0$, $\sigma_\delta = 0$, $\nu_n = 0$) we have

$$O = O_\delta = O_{1_i} = O_2 = O_3 = D^2 - a^2$$

and the dispersion equation (26) can be reduced to the form

$$[O(O^2 - QD^2)^2 + (O^2 - QD^2)(Ra^2 - Sa^2)]W = -U(V + 2D^2 + a^2)^2 O^2 D^2 W \tag{27}$$

where $O^2 = (D^2 - a^2)^2$
Consider the case of a plasma layer with two free surfaces Then the boundary conditions at $z = 0$ and $z = d$ are

$$W = D^2 W = 0, \ \Theta = \Gamma = X = DZ = 0$$

The proper solution of equation (26) characterizing the lowest mode is

$$W = E_0 \sin(\pi z) \tag{28}$$

where E_0 is a constant
Substituting (28) in (27) and letting $x = a^2/\pi^2$, $R_1 = R/\pi^4$, $S_1 = S/\pi^4$, $Q_1 = Q\pi^4$, $V_1 = V/\pi^2$, we obtain the modified Rayleigh number R_1

$$R_1 = \left(\frac{1 + x}{x}\right)[(1 + x)^2 + Q_1] + U\frac{[V_1 - (2 - x)]^2(1 + x)^2}{x[(1 + x)^2 + Q_1]} + S_1, \tag{29}$$

where $x = (a/\pi)^2 = (kd/\pi)^2$
This relation is identical with the relation obtained by Gupta and Singh [4]. From (29) we obtain

$$\frac{dR_1}{dV_1} = U\frac{A \quad 2(V_1 - B)}{x(A + Q_1)}$$

$$\frac{dR_1}{dU} = \frac{A \quad (V_1 - B)^2}{x(A + Q_1)}$$

$$\frac{dR_1}{dS_1} = 1,$$

where $A = (1 + x)^2$, $B = 2 - x$ We observe, $dR_1/dV_1 > 0$ for $x \geqslant 2$, so that, for $x \geqslant 2$, the effect of rotation is always for the stabilization of the system and $dR_1/dU > 0$, $dR_1/dS_1 > 0$ for all values of V_1 and x The FLR effects and solute gradient have a stabilizing influence on the thermosolutal instability.

REFERENCES

1 R C Sharma, K Prakash, S N Dube, Acta Phys Acad Sci Hung **40**(I), 3(1976)
2 M Vasiu, vol *Progrese în Fizică*, ICEFIZ, 5—7 octombrie, Oradea, 559 (1989), Studia Univ Babeş-Bolyai, Cluj, Physica, **33** (1), 21 (1988)
3 M Vasiu, vol lucr 1-st Gen. Conf Balkan Phys Union, 26—28, Sept, 1991 Thessaloniki, Greece
4 P N. Gupta, K V Singh, Contrib Plasma Phys **26**(5), 353 (1986)

STUDIA UNIV BABEŞ-BOLYAI, PHYSICA, XXXVI, 1, 1991

ISOTOPE ANALYSIS OF MARS GASEOUS COMPONENTS

DUMITRU RISTOIU,* DANIEL URSU,** NICOLAE LUPŞA,** NICOLAE GLIGAN** VADIM GLEBOVICI ISTOMIN***

ABSTRACT. In the case of Mars, as well as in the case of the other planets, the knowledge of the atmosphere composition and especially of isotopic ratios is very useful for the explanation of the genesis and evolution of the atmosphere The importance of the physical and chemical processes which are playing a major role in the state of the atmosphere, can be outlined by isotopic data

The mass spectrometry is the most important and versatile method for isotopic ratios measurements Taking account of the advatanges of quadrupole mass spectrometers [1,2] and those of double collectors magnetic mass spectrometers, a twin quadrupole mass analyser device is presented

Introduction. The use of mass spectrometers devices in the planetary missions was very useful for the study of planetary atmospheres of the Earth, Venus, Mars and Jupiter [3—6]

Very valuable, for the trends of explanations of the evolution of the whole planetary system and of the planetary atmospheres, are the isotopic data.

Taking account of the accuracy of double collector methods, used for the mass spectrometer isotopic analysis, a device consisting of twin quadrupole mass spectrometers is presented.

The device. The double collector method is realised by the simultaneous use of a pair of quadrupole mass spectrometers Such a mode of operation of the device can resolve some problems like those appearing in the case of quick commutation of the range of ionic current measuring systems, quick temporary variations of the pressures and bulk variations of the electronics.

The construction of the device is presented in Fig 1

The geometry of the twin quadrupole mass spectrometers is identical

In order to tune one of the quadrupolar mass spectrometer on the mass m the potentials $\pm(U + V \cdot \cos \omega t)$ are applied on the rods of mass analyzer For given a and q — operating parameters — the magnitude of U and V can be deduced from the relations [7]

$$a = \frac{8eU}{mr_0^2w^2} \qquad q = \frac{4eV}{mr_0^2w^2}$$

In these relations e — electron charge, r_0 — radius of the quadrupole field, w — operating frequency of the mass analyser

For the tuning of the other quadrupole mass spectrometer, on the mass $m + k$ the potentials $(U' + V' \cos wt)$ must have $U' = U(1 + k/m)$ and $V' = V(1 + k/m)$

Until the contributions of the ions having masses $m + k - 1$ and $m + k + 1$ does not give remarkable contributions to the peak of the ions of mass $m + k$, one can decrease the mass resolutions in order to obtain higher ionic currents

The operations of device is done and controlled by microcomputerized electronic unit.

The microcomputerized electronic unit (Fig 2) consists from

— power supply of the ion sources (ASI),

— two identical radiofrequency generators (GRF_1, GRF_2),

— pilot oscillator (OP),

* *University „Babeş-Bolyai", Department of Physics, 3400 Cluj-Napoca, Romania*
** *Institute of Isotopic and Molecular Technology, P O Box 700, 3400 Cluj-Napoca, Romania*
*** *Space Research Institute, Moscow, C S I*

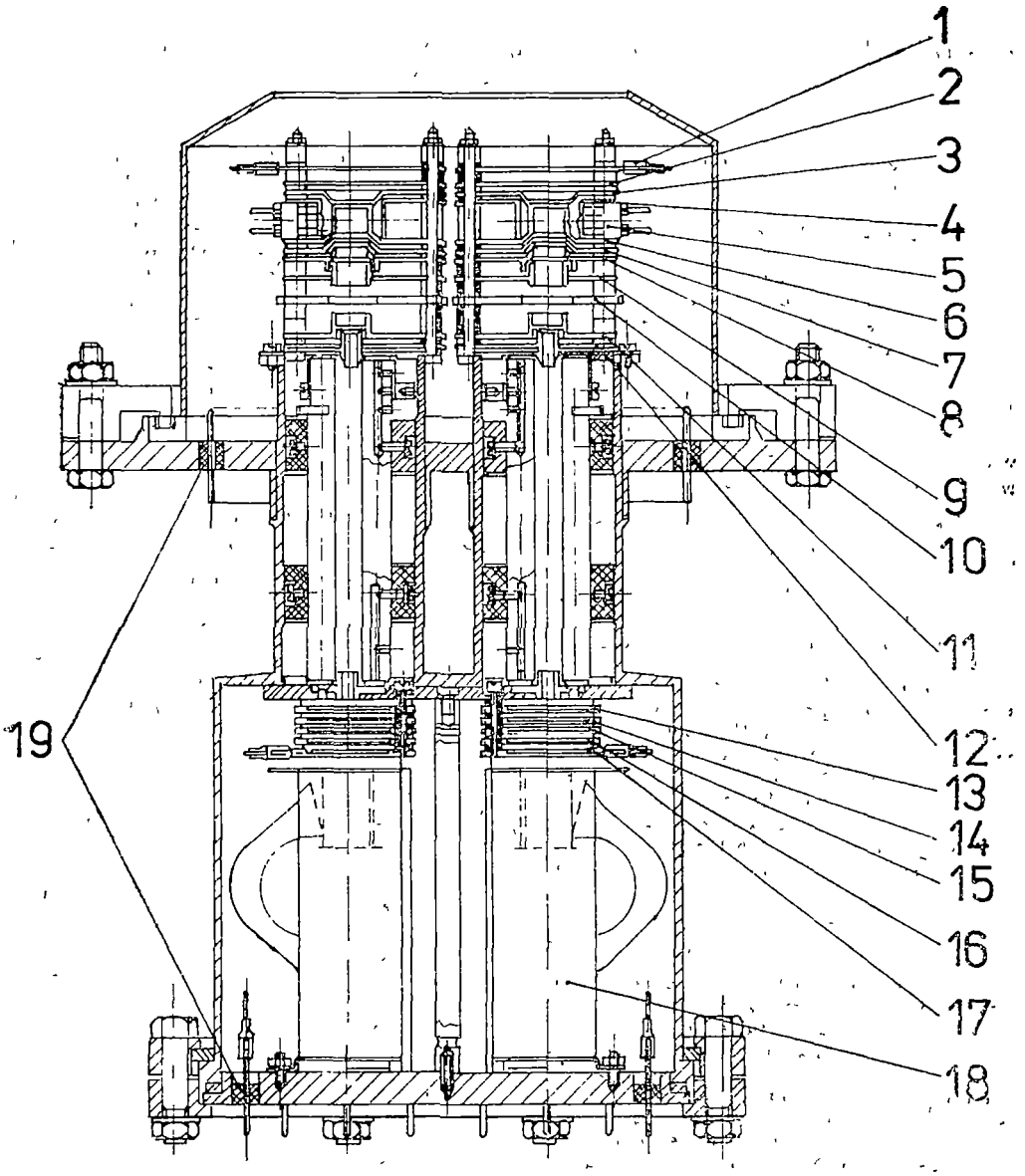

Fig 1 *The mass spectrometric device* 1, 2, 3 — grids, 4 — electron lens, 5 — filament ensemble, 6 — ionization chamber, 7 — extraction grid, 8,9 — ion lens, 10 — retarding potential analyser, 11 — total ion current collector, 12 — entrance aperture, 13, 15, 17 — screen grids, 14, 16 — ion collector grids, 18 — channeltron electron multiplier, 19 — feedthroughs

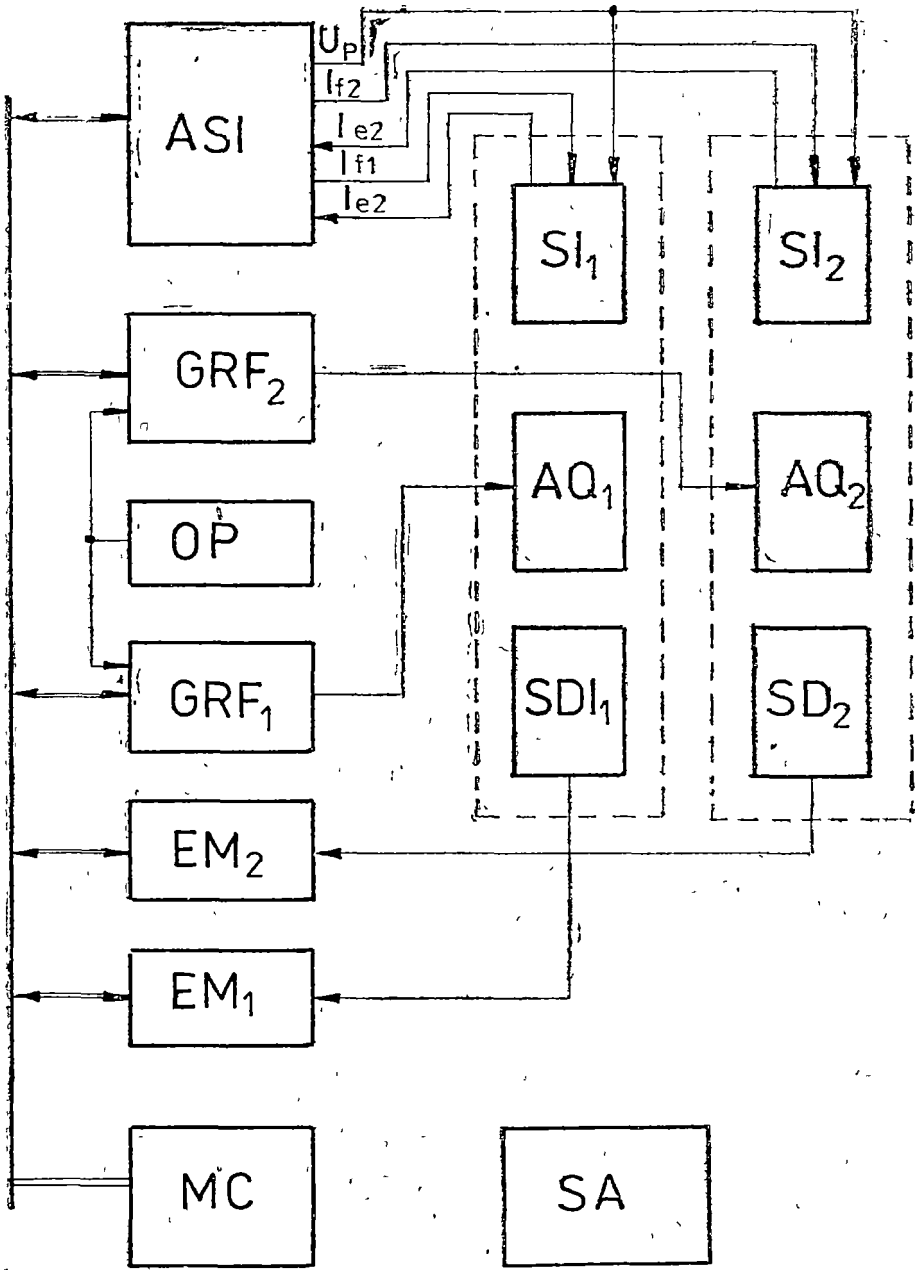

Fig 2 *Schematic diagram of the electronic unit.*

— two identical measuring channels for the ionic currents (EM_1, EM_2),
— microcomputer system (MC),
— general power supply bloc (SA)

The potentials (U) on the electrodes of the both ion sources (SI_1, SI_2) are given in parallel from common voltage sources From separate current sources are obtained the currents (IF_1, IF_2) for the filaments of the ion sources Each current source is commanded by the system of emission regulation In this mode is assured the highest identity of operation conditions for the both ion sources

Microcomputer system controls and regulates the emission current (IE_1, IE_2) and the energy of ionizing electrons (which must be identical for both ion sources)

The potentials furnished by the two radiofrequency generators, applied to the mass analysers (AQ_1, AQ_2), are controlled independently by the microcomputer system, in such a manner that a mass analyser is tuned on mass m and the other on mass $m + k$

The ionic currents, detected by the collecting systems (SDI_1, SDI_2) are measured by electrometric systems (EM_1, EM_2), and the values are fed to the microcomputer system for future processing of data.

Bassed on stored programs, the microco mp uter system can assure the commutation of the device on ionic or on neutral mode of operation In ionic mode, one measures the ionic components of atmosphere, the filaments of the ion sources being cut-off Also the microcomputer system assures the choice of scan mode for both quadrupole mass spectrometers This mode is useful for diagnostic of operation and also for collection of informations relating the composition of atmosphere By telecomands there is the possibility for the installation of other modes (not previously installed) of operation of the device.

Considerations on isotopic measurements. During the preparation for Mars missions, in order to test the apparatus, it must be exploited in simulated martian atmosphere Taking account of the acquired data by Mariner — 4, Mariner 9, Viking —1, Viking —2, Mars —2, Mars —3, Mars —5 and Mars —6, [8—10], was considered a Mars atmosphere composition like that presented in Table 1.

In Table 2 are presented the mass spectra of the most important components of martian atmosphere The spectra are calculated for the case of terrestrial isotopic abundances. In the last column, under the name Sp M is presented a composite mass spectrum by combining the data given in Table 1 and 2 The data of Table 2 are showing that there are many superpositions of different fragment ions at the same m/z

Lowering the energy of ionizing electrons, one could obtain only the most abundant ions of mass spectra [10] In these conditions one can avoid a lot of superpositions and consequently the mass spectra are much simpler Such mass spectra are shouwn in Table 3 In Table 4 are pressented the ionization potentials of considered components

Taking account of the ionizing potentials, on remaiks for 0.5 eV spread of electrons energies, that for electron energy of about

— 10 eV, one obtains peaks at the masses 142 and 143 for CH_3I, 34 and 35 for PH_3, 93—96 for CH_3Br, and 94—97 for CH_2Br_2 Assuming that the martian iodine and phosphor, are monoisotopical, one can deduce the ratio H/D Bassed on the ratio H/D, considering the peaks from the range 93—97 one can obtain informations on bromide isotopes Despite of very low concentrations of implied neutral species, there is the chance of almost equal concentrations;

— 11.5 eV one obtains peaks at the masses 50—53 for CH_3Cl, 49—52 for CH_2Cl_2 and 80—82 for HBr The reduction of these data permits to obtain useful informations about chlorine and bromide isotopes,

Table 1

The abundances of some components of martian atmosphere

C	C02	N2	Ar	02	HBr	CO	H2O	CH3C1	CH31	PH3	CH3Br	CH2C12	CH2Br2	HCN	N20
[%]	93	4	2	13	1	07	06	005	004	003	003	003	.002	.001	001

Table 2

The „terrestrial„ mass spectra of the components of the martian atmosphere

m/z	C02	N2	Ar	02	HBr	CO	H20	CH3Cl	CH3I	PH3	CH3Br	CH2C12	CH2Br2	HCN	N2O	Sp *M*
1					14			01		02						.0002
2					7 00			58		1 00						.0076
12	2 77					4 71		3 30	05		50	2 90	4 19			2 7724
13	03					05		5 44	61		91	5 53	1 74			.0315
14		5 20						8 46	95		2 11	9 36	1 67		12 98	2245
15		02						72 38	12 81		46 62	11	01		05	0068
16	6 35			5 13		1 72	90	84	15		54				5 04	6 3617
17							21 20									0161
18	01			01			∗100∗								01	0775
19							11									
20							20									0001
26													16 60			0002
27													∗100∗			0011
28	6 55	∗100∗				∗100∗							1 50		10 83	10 926
29	08	74				1 16									08	1083
30	01					21									31 22	0140
31										32 10					13	0012
32				∗100∗						12 70					.06	1402
33				08						33 10						0012
34				.41						∗100∗						0038
35								6 20		04	11 57					0007
36			34					1 60			2 10					0074
37								1 98			3 70					0002
38			06					51			67					0014
40			∗100∗													2 1505
44	∗100∗														∗100∗	100
45	1 20														77	1 1954
46	41														.21	4093

Table 2 (continued)

The ,,terrestrial,, mass spectra of the components of the martian atmosphere (continued)

m/z	CO2	N2	Ar	O2	HBr	CO	H2O	CH3Cl	CH3I	PH3	CH3Br	CH2Cl2	CH2Br2	HCN	N2O	Sp *M.*
47	,01							7.10				16.83				.0057
48								3.44				8 43				0009
49								13 57				∗ 100 ∗				.0040
50								∗ 100 ∗				3 78				.0055
51								4 76				30 26				.0012
52								31.63				.35				.0017
53								.37								
79					45 01						6.12		27.40			.0492
80					∗ 100 ∗						1 55		3 71			.1077
81					43 80						5 95		26 66			.0479
82					97 29						1 51	.59	3.61			.1048
83					01							1 90				
84												58.10				0019
85												1 88				
86												36 98				.0012
87												62				
88												5 90				.0002
89												0 7				
91											6.53		12.93			.0005
92											3 91		5 30			0002
93											26 45		∗ 100 ∗			0030
94											∗ 100 ∗		6 16			0034
95											20.68		85 05			0025
96											93 59		98			0030
97											1 09					
127									37 80							0016
128									2 73							0001
139									4 50							0002
140									3 97							0002
141									14 12							0006
142									∗ 100 ∗							0043
143									1.16							
158													.77			
160													3 04			
162													3 73			
164													1 46			
170													21			

Table 2 (continued)

The ,,terrestrial,, mass spectra of the components of the martian atmosphere (continued)

m/z	CO2	N2	Ar	O2	HBr	CO	H2O	CH3C1	CH3I	PH3	CH3Br	CH2C12	CH2Br2	HCN	N2O	Sp *M*
171													31			
172													23 94			0005
173													88			
174													46 00			0010
175													82			
176													22 28			0005
177													.26			

Table 3

The ,,mass spectra,, of the principal ions

m/z	CO2	N2	Ar	O2	HBr	CO	H2O	CH3C1	CH3I	PH3	CH3Br	CH2C12	CH2Br2	HCN	N2O
18							*100*								
19							.066								
20							204								
27														*100*	
28		*100*				*100*								1 503	
29		735				1 158								004	
30		.001				.205									
31						002									
32			*100*												
33			.075												
34			.409								*100*				
35										.044					
36			.338												
38			063												
40			*100*												

Table 3 (continued)

The „mass spectra„ of the principal ions (continued)

m/z	CO2	N2	Ar	O2	HBr	CO	H2O	CH3C1	CH3I	PH4	CH3Br	CH2C12	CH2Br2	HCN	N20
44	∗100∗														∗ 100∗
45	1 195														773
46	410														206
47	005														002
49												∗100∗			
50								∗100∗				1 149			
51								1 164				31 978			
52								31 978				368			
53								.368							
80					∗100∗										
81					.015										
82					97 293										
83					014										
93													∗100∗		
94											∗100∗		1 149		
95											1 164		97 293		
96											97 29		1 118		
97											1 132				
142									∗100∗						
143									1 162						

Table 4

The ionization potentials of the principal ions

C	CO2	N2	Ar	O2	HBr	CO	H2O	CH3C1	CH3I	PH3	CH3Br	CH2C12	CH2Br2	HCN	N2O
[eV]	13 79	15.51	15 79	12 2	11.62	14.01	12 56	11 17	9 49	9 98	10 49	11 35	10 49	13 57	12.9

— 12 5 *eV* one obtains peaks at masses 32—34 for O_2, 18—20 for H_2O and 44—47 for N_2O The reduction of these data permits to obtain useful informations about oxygen and nitrogen isotopes,

— 13 5 *eV* one obtains peaks at masses 27—29 for HCN, 44—47 for CO_2 and 28—31 for CO Due to the very high concentration of CO_2 only informations about carbon and oxygen isotopes can be deduced

REFERENCES

1 D Ristoiu, N Lupşa and D Ursu, 12-th International Mass Spectrometry Conference, Amsterdam 1991
2 Toderean, G, Ristoiu, D, Mercea, V, Istomin, V, Rev Roum Phys, **24** (1979), 685
3 Niemann H B, Kasprzak W J, Hedin A E, Hunten D M, Spencer N W, J Geophys Res **85** (1980) 7817
4 Istomin V G, Grechnev K V, Kotchnev V A, Space Research Vol **XX** (1980), 215
5 Kondratyev K Ya, *Planet MARS*, Leningrad, Gidrometeoizdat, 1990
6 Sakimura M, *Mass Spectroscopy* **18** (1970), 1077
7 Niemann, H B, Proc Int Workshop, ESA SP—241, 1985
8 Niemann, H B, Both, J R., Cooley, J E, Hartle, R E, Kasprzak, W T, Spencer, N W, Way, S H, Hunten D M, and Carignan, G R, IEEE Trans. Geosci. Rem Sens, GE—**18** (1980), 60
9 Niemann, H B, Kasprzak, W T, Hedin, A E, Hunten, D M, and Spencer, N W, J Geophys Res, **85** (1980), 7817
10 Nier, A D, McElroy M B, J Geophys Res **82** (1977) 4341

STUDIA UNIV BABEŞ-BOLYAI, PHYSICA, XXXVI, 1, 1991

EFFECT OF THE MAGNETIC CORRELATIONS ON THE SPECIFIC HEAT OF THE 2D HIGH TEMPERATURE SUPERCONDUCTORS

I. GROSU

ABSTRACT. The influence of the magnetic correlations in a two-dimensional Fermi liquid is considered in order to find the low temperature specific heat The specific heat has two terms corresponding to the electronic and the lattice part The electronic specific heat has been calculated taking into consideration the electronic mass enhancement due to the spin fluctuations The low-temperature lattice part behaves like T^2

Introduction. It is well known that the enhancement of the electronic mass in the Fermi systems appears due to the interactions of the electrons with different excitations as phonons, spin fluctuations, (paramagnons), or with localized spins In the low temperature limit, the electronic part of the specific heat is given by

$$C_e = \gamma T = \frac{m^*}{m} \cdot \gamma_0 T \tag{1}$$

where γ_0 is the Sommerfeld constant of a two-dimensional non-interacting system The evaluation of the enhanced mass m^* will be performed using the formula

$$\frac{m^*}{m} = 1 - \frac{\partial}{\partial \omega} \sum (P_F, \omega)\Big|_{\omega \to 0} \tag{2}$$

where $\sum(p_F, \omega)$ is the self-energy of the electrons, interacting with the spin fluctuations Using (2) in (1), a complete formula of the electronic specific heat will be determinated The result will contain corrections due to the spin fluctuations The lattice part will be performed using a standard procedure

Effective electronic mass and electronic specific heat. Using the standard many-body method proposed by F u l d e [1], the electronic self-energy will be

$$\sum(\vec{p}, i\omega_n) = -\frac{g^2}{\beta} \sum_m \int \frac{d^2\vec{p}'}{(2\pi)^2} \cdot G(\vec{p}', i\omega_m) \cdot R(\vec{p} - \vec{p}', i\omega_n - i\omega_m) \tag{3}$$

g = the coupling constant between electrons and the spin fluctuations.

$\beta = \frac{1}{K_B T}$, K_B — the Boltzmann constant.

$G(\vec{p}', i\omega_m)$ the Green function of an interacting electronic system.

$R(\vec{p} - \vec{p}', i\omega_n - i\omega_m)$ the bosonic propagator.

* University „Babeş-Bolyai", Department of Physics, 3100 Cluj-Napoca, Romania

Using the spectral representation

$$G(\vec{p}', \imath\omega_m) = \int_{-\infty}^{+\infty} dE \cdot \frac{S(\vec{p}', E)}{\imath\omega_m - E} \tag{4}$$

$$R(\vec{p} - \vec{p}', \imath\omega_n - \imath\omega_m) = \int_{-\infty}^{+\infty} dE' \frac{r(\vec{p} - \vec{p}', E')}{\imath\omega_n - \imath\omega_m - E'} \tag{5}$$

and considering

$$S(\vec{p}', E) \sim \delta(E - E_{p'}) \tag{6}$$

$$E_{p'} = \varepsilon_{p'} + \mathrm{Re}\ \Sigma \tag{7}$$

$$r(\vec{q}, E') = -\frac{1}{\pi} \cdot Im R(\vec{q}, E') \tag{8}$$

we find.

$$\frac{m^*}{m} = 1 - g^2 N(0) \cdot \frac{\beta}{2\pi^2 p_F} \int_0^{2p_F} \frac{dq}{\pi} \int_0^{\infty} dz \cdot Im R(q, z) \cdot Re\left[\imath\Psi'\left(\frac{1}{2} + \imath\frac{\beta z}{2\pi}\right)\right] \tag{9}$$

where p_F — the Fermi momentum
Ψ — the digamma function
an the case of the spin fluctuations formula (9) and the t-matrix method gives In alternative expression

$$\frac{m^*}{m} = 1 - N(0) \frac{\beta}{2\pi^2 p_F} \int_0^{2p_F} \frac{dq}{\pi} \int_0^{z_c} dz \cdot Im t(q, z) \cdot Re\left[\imath\Psi'\left(\frac{1}{2} + \imath\frac{\beta z}{2\pi}\right)\right] \tag{10}$$

Here

$$t(q, z) = -U^2 \cdot Im\chi(q, z) \tag{11}$$

where U-is the Coulomb interaction and χ is the dynamical susceptibility In the Random Phase Approximation ($R\,P\,A$) [2] the dynamical susceptibility of a 2D Fermi system is

$$\chi(q, z) = \frac{\chi_0(q, z)}{1 - U\chi_0(q, z)} \tag{12}$$

The imaginary part of χ_0 has been calculated as [3].

$$Im\chi_0(q, z) = N(0) \frac{z}{v_F q \sqrt{1 - \left(\frac{q}{2p_F}\right)^2}} \tag{13}$$

From (11—13) we get

$$Im\, t(q, z) = -\frac{N(0)U^2 \quad z}{v_F q \sqrt{1 - \left(\frac{q}{2p_F}\right)^2}} \cdot \left[(1 - UN(0))^2 + \left(\frac{N(0)Uz}{v_F q}\right)^2 \cdot \frac{1}{1 - \left(\frac{q}{2p_F}\right)^2}\right]^{-1} \tag{14}$$

Now using (14) in (10)

$$\frac{m^*}{m} = 1 + \left[\frac{UN(0)}{2\pi(1 - UN(0))}\right]^2 \cdot \frac{\beta}{2\pi E_F} \int_0^{z_c} dz \cdot z \; Re\left[i\Psi'\left(\frac{1}{2} + i\frac{\beta z}{2\pi}\right)\right] \times$$

$$\times \left[\left(\frac{1}{\sqrt{1+A}} + 1\right)\frac{1}{\sqrt{2}} \cdot \frac{1}{\sqrt{1+\sqrt{1+A}}} \cdot \ln \frac{\frac{1}{2}(1+\sqrt{1+A}) + \frac{1}{\sqrt{2}}\sqrt{1+\sqrt{1+A}}}{\frac{1}{2}(1+\sqrt{1+A}) - \frac{1}{\sqrt{2}}\sqrt{1+\sqrt{1+A}}} - \right.$$

$$\left. - \left(\frac{1}{\sqrt{1+A}} - 1\right) \cdot \sqrt{2} \cdot \frac{1}{\sqrt{\sqrt{1+A} - 1}} \cdot \operatorname{arctg} \frac{\sqrt{2}}{\sqrt{\sqrt{1+A} - 1}}\right] \qquad (15)$$

where:

$$A = \left[\frac{UN(0)\; z}{2E_F(1 - UN(0))}\right]^2 \qquad (16)$$

From (15) the electronic mass m^* decreases as the temperature T increases and from here:

$$C_e = \gamma_0 \frac{m^*}{m} \cdot T = \gamma(T) \cdot T \qquad (17)$$

Two-dimensional lattice specific heat. Using the Debye method the specific heat of a two-dimensional periodic crystal lattice containing N identical atoms at low temperature varies with temperature as T^2. Indeed

$$C_l = \frac{dU}{dT} \qquad (18)$$

with

$$U = \int_0^{\omega_D} \frac{1}{e^{\frac{\hbar\omega}{K_B T}} - 1} \cdot \hbar\omega \cdot g(\omega) \; d\omega \qquad (19)$$

and $g(\omega) = \frac{S \cdot \omega}{\pi V^2}$, where S is the area of the crystal (is chosen to be unity). Thus in the low temperature limit

$$C_l = 24\zeta(3) \cdot N \cdot K_B \; \frac{T^2}{\theta_D^2} \sim T^2 \qquad (20)$$

where $\zeta(n)$-is the zeta Riemann function and

$\theta_D = \frac{2\hbar v\sqrt{\pi n}}{K_B}$, $n = \frac{N}{S}$ — is the Debye temperature of a two-dimensional crystal.

Conclusions. The specific heat of a $2D$ high T_c superconductor was calculated in the low temperature limit. We find that

$$C = C_e + C_l = \gamma(T) \cdot T + AT^2 \qquad (21)$$

with a temperature dependent „effective Sommerfeld constant" The temperature dependence of the „Sommerfeld constant" is connected with the temperature dependence of the effective electronic mass, which decreases with temperature in agreement with ciclotronic resonance and heat capacity measurements

REFERENCES

1. P. Fulde, J Jensen, Phys Rev **B, 27,** 4085, (1983).
2 S. V. Vonsovsky, Y A Izyumov, E Z Kurmaev, *Superconductivity of Transition Metals* Springer Verlag, Berlin, Heidelberg, 1982
3. H. Theumann, M T Beal-Monod, Phys Rev **B, 31,** 2764, (1985).

STUDIA UNIV BABEŞ-BOLYAI, PHYSICA, XXXVI, 1, 1991

THE FRACTAL STRUCTURE OF THE ZEROSETS

Z. GINGL*, Z. NEDA**

ABSTRACT. We studied the fractal properties of the zerosets for 1, 2 and 3 dimensional random walks on square-type lattices We obtained the same $D = 0.5$ dimensional fractal structure in 1 and 3 dimensions, and a totally different behaviour in 2 dimensions $d = 3$ is a critical dimensions, for the zerosets.

1. **Introduction.** The aim of our paper is to study the fractal dimension of the zerosets generated by random walks on 1 dimensional $(1d)$, 2 dimensional square $(2d)$, and 3 dimensional cubic lattices $(3d)$ We define zeroset as the set containing the time-moments in which our particle intersect the origin For an infinite random motion this set could have a fractal structure on the real axis, characterized by a $D(0 \leq D \leq 1)$ fractal dimension. We proposed to determine this D fractal dimension.

2. **The Method.** Taking account that our motions on the chosen lattices will be in discrete steps we must use the number of steps as the time variable One can immediately observe that a particle might be back in the origin only after even number of steps The D fractal dimension will be calculated by examining the length distribution of the intervals between the points of the zeroset, using the following theorem [6]

THEOREM The distribution of empty regions (holes) in a fractal of dimension D, scales as a function of their linear size with an exponent $-D-1$. The statement is essentially the following.

$$n(\varepsilon, \Delta\varepsilon) \sim \varepsilon^{-D-1} \cdot d\varepsilon, \tag{1}$$

where $n(\varepsilon, \Delta\varepsilon)$ is the number of gaps (empty regions) of length between ε and $\varepsilon + \Delta\varepsilon$

The length distribution of the intervals between the points of the zeroset will be studied analytically $(1d)$ and numerically using the following recursion formula.

$$Q(N) = P(N) - \sum_{i=1}^{N-Z} Q(i) \cdot P(N-i), \tag{2}$$

where

$Q(i)$: is the probability of returning first time in the origin exactly after i random steps,

$P(i)$. is the probability of finding the particle in the origin after i random steps.

* *József Attila University, Szeged, Hungary*
** *Babeş-Bolyai University, Cluj, Romania*

Using simple combinatorics we found the $P(i)$ values for our lattices Now with $Q(2) = P(2)$, and with equation (2) we are able to study $Q(N)$. From equation (1) we have

$$Q(N) \sim N^{-D-1}, \tag{3}$$

and so for $N \gg 1$ we can determine the possible D fractal dimensions

3 **The 1*d* case.** For the 1 dimensional random walk

$$P_1(N) = \frac{\binom{N}{N/2}}{2^N}, \tag{4}$$

and using equation (2) we established an analytical result for $Q_1(N)$

$$Q_1(N) = \frac{1}{N} \cdot \binom{N-2}{N/2-1} \cdot \frac{1}{2^{N-2}} \tag{5}$$

Now it is easy to study analytically and numerically the asymptotical behaviour of $Q_1(N)$ Logarithming (5) and using the Stirling formula, we found for $N \gg 1$ that

$$Q_1(N) \sim N^{1.5}, \tag{6}$$

and so

$$D_1 = 0.5 \tag{7}$$

In accordance with the known literature results [2], [7] we got the $D_1 = 0.5$ value for this fractal dimension

4 **The 2*d* case.** For this random walk we have

$$P_2(N) = \frac{1}{4^N} \binom{N}{N/2}^2 = P_1(N)^2 \tag{8}$$

Unfortunately we did not find any analytical result for $Q_2(N)$, and so we studied it only numerically

Examining the $[\ln Q_2(N) - \ln (N)]$ plot we got $-Dz(N) - 1$, in function of N. The Dz value we are looking for is the asymptotical limit of $-Dz(N) - 1$ $\{(-Dz - 1) = \lim_{N\to\infty}(-Dz(N) - 1)\}$

Now supposing that $-Dz(N) - 1$ converge as

$$-Dz(N) - 1 = (-Dz - 1) \cdot [1 - C \cdot N^{-\alpha}], \tag{9}$$

we can determine C, Dz and α with the Gaussian best fit method We reached to calculate $Q_2(N)$ until $N_{max} = 60\,000$, but the convergence was still very weak ($\alpha < 0.2$) The best values we obtained on the $[N_{max}/2, N_{max}]$ interval were $\alpha = 0.1315$ and $Dz = 0.0684$ From this results, we conclude only that for $N < 60\,000$ the zeroset of a $2d$ random walk cannot be approximated as a simple Dz dimensional fractal, because $Dz(N)$ is not constant even for large N For the $N \to \infty$ asymptotical limit our results suggest only that Dz must be smaller than 0.07!

5 **The 3*d* case.** In a cubic lattice

$$P_3(N) = \frac{1}{6^N}\begin{bmatrix} N \\ N/2 \end{bmatrix} \cdot \sum_{k=0}^{N/2} \begin{bmatrix} N/2 \\ k \end{bmatrix}^2 \cdot \begin{bmatrix} N-2k \\ (N-2k)/2 \end{bmatrix} \tag{10}$$

Working exactly as in 2*d*, surpisingly we found that the convergence of the $-D\varepsilon(N) - 1$ series is good even for small N and the zeroset has the same structure as in 1*d*, with the fractal dimension

$$D_3 = 0\,5 \tag{11}$$

It is worthwhile noting that the convergence for $-D_3(N) - 1$ is even better that in 1*d*

6 **Conclusions.** We conclude that after four results, the zeroset of the 1*d* and 3*d* random walks has the same fractal structure with the $D = 0.5$ fractal dimension The approximation for small N of the zeroset with a $D = 0.5$ fractal is better in 3*d* It seems that $d = 3$ is the critical dimension and so for $d > 3$, $P(N)$ and $Q(N)$ will scale in the same manner

	1*d*	2*d*	3*d*
$P(N)^-$	$N^{-0\,5}$	N^{-1}	$N^{-1\,5}$
$Q(N)^-$	$N^{-1\,5}$	$(N^{-1\,068})$	$N^{-1\,5}$

Unfortunately in 2*d* the approximation of the zeroset with a *Dz* dimensional fractal is wrong for $N < 60\,000$ For the $N \to \infty$ asymptotical limit we obtained only that $Dz < 0\,07$ It would be interesting to study this problem in higher dimensions too

REFERENCES

1. B B Mandelbrot, *Fractal, Form, Chance and Dimension*, Freean, San-Francisco, 1977.
2. B B Mandelbrot, *The Fractal Geometry of Nature*, Freeman, San-Francisco, 1982.
3 Z Neda, *Fractal Properties of some Special Quasi-Random Trails*, Conference Volume of the **1-BUP**, 26—28 sept 1991 Thessaloniki, Greece.
4. L Pietronero, E Tosatti, editors, *Fractals in Physics* Proceeding of the Sixth International Symopsium on Fractals in Physics, ICTP, Trieste, Italy, North-Holland, Amsterdam, 1986.
5 A Renyi, *Probability Theory* North-Holland, Amsterdam, 1970.
6 T Vicsek, *Fractal Growth Phenomena;* World Scientific Publishing Co Pte. Ltd, 1989.
7. R F Voss, *Fractals in Nature From characterization to simulation*, from — *The Science of Fractal Images*, editors H O Peitegen, D Saupe, Springer-Verlag, 1988.

STUDIA UNIV BABEŞ-BOLYAI, PHYSICA, XXXVI, 1, 1991

INFLUENCE OF THE DRIFT ON THE ABSORPTION OF ELECTROMAGNETIC WAVES IN THE LOWER IONOSPHERE

SZŐCS GÉZA* and SZŐCS HUBA**

ABSTRACT. The absorption of the electromagnetic waves increases with increasing electron-concentration of the ionospheric layers Investigation of waves with specific wavelenght yields valuable information on the state of the ionospheric layers The $A-3$ method at 185 *kcps* frequency has been applied in our observation Relationships between variation of the monthly averages of L' absorption coefficient and the magnitude and direction of the ionospheric drift were studied using correlation analysis

Electron concentration of the ionosphere is described by the continuity equation

$$\partial N/\partial t = q - kN^2 - \operatorname{div}(N\vec{v}),$$

where t is the time, N the electron concentration, q and k coefficients of origin and recombination of charges respectively, and $\vec{v}$ the velocity of convection. All these factors are hardly foreseen, the term $\operatorname{div}(N\vec{v})$ which is characteristic for the charge transport, has a special importance Hance the drift (i e the charge transported by the effect of the geomagnetic field) plays an important use in the electron concentration

The relationship between the drift and the absorbtion of electromagnetic waves has been analysed Wave absorption increases with predetermined wave length field information and the condition of the lower ionosphere.

In our studies the $A-3$ method was applied, which is based on the reflexion of the electromagnetic waves at increased incidence Absorption of very long and long waves is characteristic for the lower und upper layers of the lower ionosphere, respectively Monthly averages of L' absorption was considered for increased incidence of waves with $f = 185\ kHz$(wave length $= 1622m$). The transmitter was the Deutschlander, while the receiver was the Kuhlungsborn ($53.4°N$ and $12\,6°E$) The surface distance between the transmitter and receiver was 195 *km* Measurement of absorption was determined at night between 100 grades solar zenith and 23 30 *UT*, while measurement of $v(ms^{-1})$ and the inclination angle Ø characteristic for the drift was determined between 23 and 23 30 *UT*

The monthly averages of $L(dB)$ $1\mu V/m$, the declination angle Ø for 1969, the number of days of drift measurement and v monthly averages of drift velocity are given in Table I

* „Eszterházy Károly" Pedagogical College, Eger, Hungary
** „Kandó Kalmán" Technical College, Szekesfehervár, Hungary

Table 1

Nr	Month	*L* *dB*	*V* *m/s*	*U* grade	Day
1	I	—	—	—	—
2	F	22	48	64,75	20
3	M	21	40	226,75	16
4	A	22	42	186,25	20
5	M	25	44	214,11	17
6	I	25	41	185,50	20
7	I	24	45	191,05	19
8	A	24	41	172,66	14
9	S	21	44	248,21	14
10	O	19	39	230,79	19
11	N	19	42	118,50	25
12	D	22	40	123,13	24
Medial		22,18	42,40	184,98	18,20

The absorbtion v is plotted in Fig 1, while L us Ø is plotted in Fig 2 Analysis of the two graphs shows the trend of absorption and drift to be comparable. Correlation coefficient between the two series of data is 0 50

Fig 2 is a hodograph of transport velocity against the declination angle. Vector v is proportional to the section, while position is given by declination angle Ø in an East-North Coordinate System

The analysis resulted in the following *conclusions*

1 The value of correlation coefficient $r = 0\,5$ proves that the drift has a significant effect on the condition of the lower ionosphere

2 Hodograph of the drift proves that the change of monthly average of absorption is caused by a change in direction of the ionospheric drift (taking into account, that the magnitude of the velocity does not change considerably).

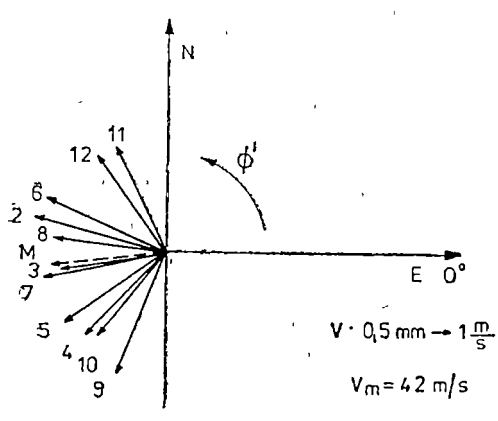

Fig 1

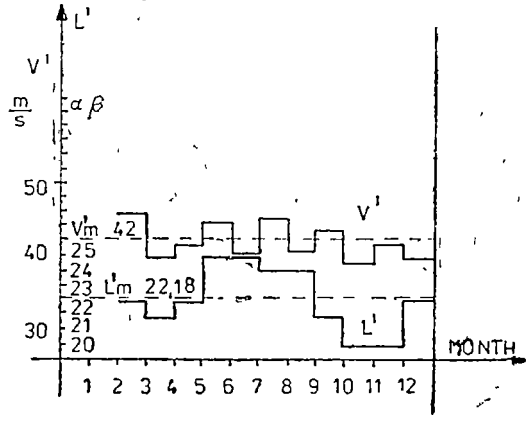

Fig 2

3. Absorption is influenced by horizontal, and vertical components of the drift.

4 In addition to the ionospheric drift motion, the electric charges are governed by the other factors That is, the lower layers of the ionosphere motion, of the electric charge is also influenced by atmospheric turbulence.

5 Multiple correlation computation renders a better understanding of the different factors influencing condition of the lower ionosphere.

Note There are two points to be mentioned about the effect of the horizontal drift on the ionospheric absorption of the radio-waves On the one hand, the effect of the horizontal drift, although it generates a vertical charge notion, is hardly demonstrated by a single resultant parameter like the absorption. On the other hand, the ionospheric absorption of radio-waves, by transaction of the electron-density, is a function of the electromagnetic radiaton of the Sun. At the observed frequency (Deutschland sender-Kuhlungsborn, 185 *kcps*) the radio-waves are reflected at a height of 90 km (*i e* at the bottom of layer *E*) where electron-density, in general, is governed by the electromagnetic radiation.

Thus the absorption varies according to the zenith distance of the Sun (except dor the winter months, due to the winter anomalies), while the drift-velocity at the described height reflects the independent motion of the neutral gases, which are able to carry the charged particles whose concentration are less at several orders of magnitude This is also proved by the direction of the drift, which (in accordance with the circulation at the level of the mezopause) is east-to-west in summer months and west-to-east in winter months.

REFERENCES

1 Bencze P, Saikó J, Szendrei J, Ionoszféra és magnetoszféra fizika **XIII**, 1986, MTSZ Budapest p 177—181
2 P R Sengupta, Space Research **XIV**, 1974, Akademische Verlag, Berlin
3 Solar Geophysical Data, 1980, NOAA Nr **435**, Part II
4. *Geophysicalische Beobatungseergebnisse Geophysical Data* 1969—1982, H, Hertz Inst Deutsche Akad der Wissenschaften zu Berlin
5 Saikó J, Ionoszféra és magnotoszféra fizika, 1985, MTESZ, Budapest p 75—92.
6 Szőcs G, Teza de doctorat 1990, Universitatea Babeş—Bolyai
7 Szőcs G, Szőcs H, Lucrările sesiunii ştiinţifice I S Bacău, 1988
8. Saiko J, *Az ionoszfera dinamikai folyamatainak vizsgálata*, Ionoszféra és magnetoszféra fizika **XVI.** MANT, 1989
9. A. Nicula, Szőcs G, Szőcs H, Studia Univ Babeş-Bolyai, Physica, XXXV vol. 2 (1990)

STUDIA UNIV BABEŞ-BOLYAI, PHYSICA, XXXVI, 1, 1991

THE SUPERRADIANT MODEL FOR *FEL*

SPERANŢA COLDEA*

ABSTRACT. A short analysis of the superradiant FEL operation is presented The case where a Stimulated Raman Backscattering *FEL* operates as an amplifier for noise is considered

1 **Introduction.** The analysis of the superradiant (or superluminiscent) FEL model is made based upon some theoretical study of the radiation produced by the interaction of an electron beam with a rippled magnetic field [1] — [3] From the intersection of the Doppler-shifted negative energy space-charge mode and the cyclotron waves (in the dispersion diagram) with the wave -guide modes of the beam, excited in a SRB—FEL, the spectrum of resulted radiation can be investigated Experimentally was established that this radiation occus in the 10—30 *GHz* spectral region Only the negative-energy (Stokes) modes are unstable, the positive-energy (antiStokes) mode being stable. The analysis is complicated by the existence of many wave-guide modes and the presence of the beam noise

2. **Discussion** Some intense submillimeter radiation produced by SRB process from a strong microwave pump field was also discovered [4] In this case we must admite that the role of the rippled field was also to produce a strong pump wave in the electron frame, we will simplify the study by considering a short ondulator (wiggler) period which permits the generation of a radiation in the millimeter frequency region

The mechanism of the superradiant process could be described as follows. the ponderomotive force of the beat wave, produced by the pump, and the growing scattered wave bunch, the space-charge of the electron beam and the pump wave scattered from the periodic space-charge fluctuation reinforce the scattered radiation [5] The present noise on the beam is amplified (the SRB process is a convective instability)

If a short-pulse, moderate dense electron beam (with 15 *ns*), $\gamma_z \cong 2$, $\omega_b/2\pi \cong 2$ *GHz*) is used, we can examine the dependence of power upon pump-amplitude Usually, in the experiments the strength of the rippled field is controlled by pulsed wigglers It was observed that the signal initially achieves a threshold, this will increase exponentially, the increasing coefficient being linear in pump-wiggler amplitude The existence of a threshold is a characteristic of the three-wave parametric processes, being related to the wave-coupling mechanism [6].

Two modes were identified experimentally. one due to scattering from the space-charge mode, and another due to scattering from the cyclotron mode [7]. The dependence of superradiant SRB upon pump amplitude is a linear one

* *University „Babeş-Bolyai", Department of Physics, 3400 Cluj-Napoca, Romania.*

The growth rate of the cyclotron mode varies as ω rather than $\omega_b^{1/2}$ and its damping rate varies as ω_b^2

If the intersection of the beam dispersion line with the wave-guide modes is near the light line, it is clear, that single resonances will be produced If γ_z and ω_c suffer a variation, the mode coupling process can be identified

The study of the dependence of scattered radiation power on the ondulator length reveales a convective instability The power of the cyclotron mode will be saturated, if the pump amplitude increases Probably the saturation nonlinear process is caused by the beam-dynamics effects

It is clear that, when $\omega_c = eB_{z0}/mc = \gamma\omega_0$ (the pump wave frequency) or $\omega_c = \omega_s = \gamma\omega_0 - \omega_b$, the efficiency of three-wave scattering will be enhanced. We could demonstrate this by considering a helical wiggler (ondulator) with the period $l = 18$ mm imposed over a small current electron beam ($\gamma_z = 2$, $I = 1$ kA), in the electron frame of motion Two resonances in scattered radiation signal should be found, when the electron gyrates in the same sens as the helical field When the B_{z0} field is reversed, no resonant effect is obtained The two resonances correspond to $\Omega_c = \gamma\omega_0$ and $\Omega_c = \omega_s = \gamma\omega_0 - \omega_b$

As a conclusion we can observ, that are many limitations in the supperradiant FEL operation the output radiation is dependent upon the noise present at the beam input into the wiggler, also the spectrum of unstable modes is larger when the gain pump amplitude is increased (the finite bandwidth is given by $\Delta\omega_s \sim Im\ \omega$), this phenomenon being observed experimentally too In the Raman regime FEL operation, the line (bandwidth) broadening mechanism is a homogeneous one

REFERENCES

1 P Sprangle, V L Granatstein and L Baker, Phys Rev **A12**, 1697 (1975).
2 W M Manheimer and E Ott, Phys Fluids **17**, 1413 (1974)
3 P C Efthimion and S P Schlesinger, Phys Rev **A 16**, 633 (1977)
4 T C Marshall, S Talmagt and P Efthimion, APPl Phys Lett **31**, 320 (1977)
5 S Coldea, Studia Univ Babeş—Bolyai, ser Physica, vol XXXV, nr 1—2 (1990)
6 S Coldea, Studii şi Cercetări de Fizică, vol 35, nr **10**, (1990)
7 R. M Gilgenbach, T C Marshall and S P Schlesinger, Phys Fluids, **22** 971, 1219 (1979)

STUDIA UNIV BABEŞ-BOLYAI, PHYSICA, XXXVI, 1, 1991

CROSS-POLARIZATION RATE USING A TIME AVERAGED PRECESSION FREQUENCY

I. ARDELEAN*

ABSTRACT. A theory based on formalism of projection operator is developed to describe the rate of thermal mixing T_{IS} between two spin species, one abundant (I), irradiated with a phase alternating radiofrequency field, and other dilute (S) The cross polarization spectra is obtained

1 **Introduction.** The introduction of the cross-polarization technique makes possible to overcome the low sensitivity of dilute spins, and provides a mean of observing the N M R signals of those nuclei in solids [1] However, this met hod cannot readily be applied to nuclei with low gyromagnetic ratios, such as, ^{57}Fe, ^{103}Rh $^{187}O_s$, ... because to achieve the H a r t m a n n - H a h n condition [2] with those nuclei, very high values of *rf* power are required

A method to reduce the *rf* power requirements for the crosspolarization of nuclei with small gyromagnetic ratios, which is based on the time average of the precession frequency, has been realized by T a k e g o s h i and M c D o w e l l [4] They have shown that by alternating the phase of the I spin locking *rf* field, the precession of an I spin isochromat around the effective field is time reversed

In order to design the efficient cross-polarization using a time-averaged precession frequency process, the understanding of the spin dynamic is essential The present paper is concerned with a particular situation of current experimental interest, one in which two different species of nuclear spins, one (I) abundant and the other (S) dilute, come to mutual equilibrium through a process of cross relaxation in a time denoted by T_{IS}

A schematic representation of the cross-polarization using the time-averaged precession frequency (CP — T A P F) is given in Fig 1 The enhancement of the S spectral line intensities is performing by cooling the I spins first $\beta_I \gg \beta_L$, and then crosspolarizing the two spin systems in order to increase β_S.

Here I spins are prepared by a $90_{\pm x}$ pulse followed by a phase-alternating spin-locking *rf* field $+Y(-Y)$, one can control the angle of precession of the I spin around the effective field in a cycle time $t_c = t_1 + t_2$ As long as the cycle time t_c of the phase alternating sequence of the I spin-locking field is short compared to the correlation time τ_c of the dipolar fluctuations in the tilted rotating frame, i e $t_c \ll \tau_c$, the apparent precession frequency of the I spin isochromat around the effective field felt by the S spins is the time average one [4]. Then the new Hartmann-Hahn condition for cross-polarization using the time-averaged precession frequency (C P — T A P F) is

$$\overline{\omega}_{eI} = \omega_{es} \tag{1}$$

* *Polytechnical Institute, Physics Department, 3400 Cluj-Napoca, Romania*

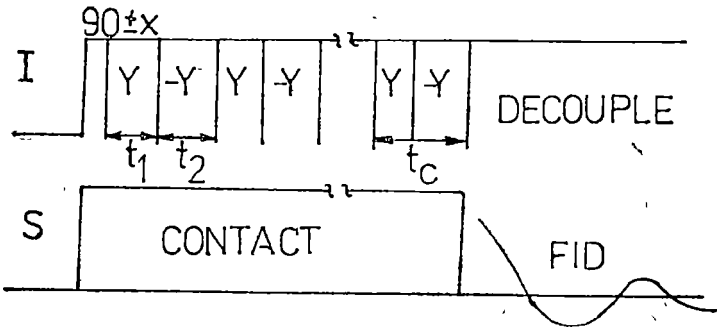

Fig 1 Pulse sequence for the CP-TAPF experiment, Y and $-Y$ represent the phases of the I spin-locking field

with $\omega_{eI} = \overline{\omega}_{eI}(t_1 - t_2)/t_c$, where $\omega_{es} = \gamma_s H_{es}$, $\omega_{eI} = \gamma_I H_{eI}$ Therefore the S spin, rf filed strength required for cross-polarization can be reduced by a scaling factor $(t_1 - t_2)/t_c \leqslant 1$ from that reguired to achieve the Hartmann — Hahn condition

2 **Hamiltonian and frame of reference.** The most common spin system encountered in the double resonance experiments contains two spin species I and S with different magnetogyric ratios γ_I and γ_s The sample, which contains N_I and N_s spins ($N_I \gg N_s$) is placed in a large static magnetic field H_0. The field H_0 is supposed to be along the Z axis We discuss only the situation in which we may neglect the relative motions of the spins, and all the spin lattice relaxation times of both spin species are taken to be infinitely long

The high field double-resonance Hamiltonian in the laboratory reference frame is

$$H = H_I + H_s + H_{Is} + H_{rf}(t) \tag{2}$$

The Hamiltonian H_I is defined as

$$H_I = H_{zI} + H_{II} \tag{3}$$

where
$H_{zI} = -\omega_{eI} I_z$, $\omega_{eI} = \gamma_I H_0$ represents the Zeeman term and H_{II} describes dipolar magnetic interaction between I spins

The Hamiltonian H_s which characterizes the dilute spin system is

$$H_s = H_{zs} + H_{ss}$$

where $H_{zs} = -\omega_{es} S_z$ Because we are interested in the behavior of spin system on a time scale small compared with the spin-spin relaxation time of the S spins, we can neglect the term H_{ss} in eq (4)

The Hamiltonian H_{Is} describes the interacion between I and S spin systems

The Hamiltonian $H_{rf}(t)$ describes the interaction of the spin system with radio-frequency magnetic field of amplitudes H_{1I} and H_{1s} and frequencies ω_I and ω_s It has the form

$$H_{rf}(t) = -2\omega_{1I} I_Y \cos \omega_I t - 2\omega_{1s} S_Y \cos \omega_s t \tag{5a}$$

for $+Y$ phase of *rf* field, and

$$H_{rf}(t) = 2\omega_{1I} I_Y \cos \omega_I t - 2\omega_{1s} S_Y \cos \omega_s t \tag{5b}$$

for $-Y$ phase *rf* filed Here $\omega_{1I} = \gamma_I H_{1I}$ and $\omega_{1s} = \gamma_s H_{1s}$, for convenience we have used in eqs (3) — (5) units in which $\hbar = 1$

The time evolution of the statistical ensemble, having an explicitly time-dependent Hamiltonian, can be described by a density operator $\rho(t)$ which satisfies the Liouville-von Newmann equation

$$i\frac{\partial}{\partial t}\rho(t) = [H, \rho(t)] = \hat{H}\rho(t) \tag{6}$$

where $\hat{H} = [H, \ldots]$ is a Liouville operator

A solution of eq (6) can be obtained if we describe the statistical ensemble in a new quantum-mechanical representation defined by the canonical transformation [5]

$$\rho_{TR}(t) = (TR)\ \rho(t)\ (TR)^+ \tag{7}$$

here

$$R = R_I R_s, \quad R_I = e^{-i\omega_I I_z t}, \quad R_s = e^{-i\omega_s S_z t} \tag{8a}$$

and

$$T = T_I T_s, \quad T_I = e^{i\theta_I I_Y}, \quad T_s = e^{i\theta_s S_Y} \tag{8b}$$

these defining „tilted rotating frames". In these reference systems the Hamiltonian of $I - S$ spin system is

$$H_{TR} = (TR)\, H\, (TR)^+ + i(\dot{TR})(TR)^+ \tag{9}$$

A concrete expression for H_{TR} can be obtained from eqs (9) and (2) — (5) in which we consider only pure dipolar coupling between the spins for $+Y$ phase, *rf* field

$$H^+_{TR} = -\omega_{eI} I_z - \omega_{es} S_z + P_2(\cos\theta_I)\, H^0_{II} + H'_p \tag{10a}$$

and for $-G$ phase *rf* field

$$H^-_{TR} = \omega_{eI} I_z - \omega_{es} S_z + P_2(\cos\theta_I) H^0_{II} + H_p \tag{10b}$$

where the effective frequencies are $\omega_{eI} = [\omega^2_{1I} - \Delta\omega^2_I]^{1/2}$ and $\omega_{es} = [\omega^2_{1s} + \Delta\omega^2_s]^{1/2}$ with $\Delta\omega_I = \omega_{0I} - \omega_I$, $\Delta\omega_s = \omega_{0s} - \omega_s$. Here H^0_{II} — zero-order average of homonuclear dipolar Hamiltonian

$$H^0_{II} = \sum_{i<j} b_{ij}(\vec{I}_i \vec{I}_j - 3I_{iz}I_{jz}) \tag{11}$$

with the interaction factor

$$b_{ij} = \gamma_I^2 \hbar\, r_{ij}^{-3} P_2(\cos\theta_{ij})$$

The Hamiltonian H_p describes $I - S$ spin interaction and at resonance it is given by

$$H_p = \sum_{i,m} b_{im} I_{i\gamma} S_{m\gamma} \tag{12}$$

with

$$b_{im} = -2\gamma_I \gamma_s \hbar r_{im}^{-3} P_2(\cos\theta_{im})$$

In the above expressions, the indices (i, j) and m refer to the I and S spins, respectively, r_{ij} is the distance between i and j spins, θ_{ij} is the angle between the vector $\vec{r}_{ij}$ connecting i and j spins and the applied magnetic field H_0. The θ_I angle is defined as $\theta_I = \mathrm{tg}^{-1}[\omega_{1I}/(\omega_{cI} - \omega_I)]$ and to resonance $\theta_I = \pi/2$

In a $CP—TAPF$ experiment we can replace the full Hamiltonian (10) by a zero order average Hamiltonian [3] defined as

$$\overline{H}^0_{TR} = \frac{1}{t_c} \int_0^{t_c} H_{TR}(t) \quad \mathrm{d}t$$

and we obtain

$$\overline{H}^0_{TR} = -\overline{\omega}_{eI} I_z - \frac{1}{2} H^0_{II} - \omega_{es} S_z + H_p \tag{13}$$

where $\overline{\omega}_{eI} = \omega_{eI}(t_1 - t_2)/t_c$ is the time averaged precession frequency in accordance with experimental results of T a k e g o s h i [4]

It is now possible to separate the spin systems involved in a double-resonance experiement into two subsystems characterized by the Hamiltonians H_I and H_s defined by

$$\begin{aligned} H_1 &= -\overline{\omega}_{eI} I_z - \frac{1}{2} H^0_{II} \\ H_2 &= -\omega_{es} S_z \end{aligned} \tag{14}$$

coupled by a Hamiltonian given by (12)

3 **The computation of cross-relaxation rate.** The spin systems, which participate in a double resonance experiment, can be described by their thermodynamic coordinates which are represented by the quantum-mechanical average of the observable operators. The time evolution of the thermodynamic coordinates as a function of the condition of experimental preparation and the physical characteristics of the subsystems can be obtained from the Liouville- von Newmann equation (6) for the density operator of the whole system

In a double-resonance experiment, the subsystems are represented by I and S spin systems The thermodynamic coordinates are defined by the quantum-mechanical averages of the operators

$$\begin{aligned} \langle H_1 \rangle_t &= T_r\{H_1 \rho_{TR}(t)\} \\ \langle H_2 \rangle_t &= T_r\{H_2 \rho_{TR}(t)\} \end{aligned} \tag{15}$$

An exact kinetic equation for the thermodynamic coordinates defined by eq. (15), has been derived in an elegant manner using ortogonal operator expansion [5] and projection operator technique The ortogonality of the operators is defined in the following sense

$$T_r\{H_1 H_2\} = 0 \tag{16}$$

Defining the projection operator P on the subspaces of Hamiltonian operators H_1 and H_2 are.

$$P = \frac{H_1}{T_r\{H_1^2\}} T_r\{H_1 \ \ldots\} + \frac{H_2}{T_r\{H_2^2\}} T_r\{H_2 \ldots\} \tag{17}$$

From eqs. (6), (10), (13), (15) for kinetic equation we obtain

$$\frac{\partial}{\partial t}\langle H_\imath\rangle_t = -\imath\, T_r\{H_1 \hat{\hat{H}}^0_{TR} P \rho_{TR}(t)\} - \imath T_r\{H\imath\, \hat{\hat{H}}^0_{TR} \bar{S}(t)\ (1 - P)\ \rho_{TR}(0)\} -$$

$$- \int_0^t d t' T_r\{H\imath\, \hat{\hat{H}}^0_{TR} \hat{S}(t - t')\ (1 - P)\ \hat{\hat{H}}^0_{TR} P \rho^0_{TR}(t')\} \tag{18}$$

where $\imath = 1, 2$ and

$$\hat{S}(t) = e^{-\imath(1-P)\hat{\hat{H}}^0_{TR} t} \tag{19}$$

is propagator and in the lowest Born approximation we can consider tha $S(t) \cong S_0(t)$. We assume here that the spin systems are prepared so that the initial density operator has a high-temperature canonical form

$$\rho_{TR}(0) \cong (1 - \beta_1 H_1 - \beta_2 H_2)/T_r\{1\} \tag{20}$$

where β_1 and β_2 are inverse spin temperatures

In the second-order approximation of the perturbation Hamiltonian when a fast-correlation assumption is introduced for times $t \gg \tau_c$ the limit in the integral of eq. (18) can be replaced by infinity and we obtain

$$\frac{\partial}{\partial t}\langle H_\imath\rangle_t = -\int_0^\infty d\tau T_r\{H_\imath \hat{\hat{H}}^0_{TR} \hat{S}_0(\tau)\ (1 - P)\ \hat{\hat{H}}^0_{TR} P\ \rho_{TR}(t)\} \tag{21}$$

Suppose now that we are interested in the cross-polarization dynamics of dilute spins. From eq (21) the following equation can be written in this case

$$\frac{\partial}{\partial t}\langle H_2\rangle_t = \frac{\langle H_2\rangle_t}{T_r\{H_2^2\}} \int_0^\infty d\tau\, C(H_2; H_2, \tau) + \frac{\langle H_1\rangle_t}{T_r\{H_1^2\}} \int_0^\infty d\tau\, C(H_2, H_1, \tau) \tag{22}$$

where the correlation functions are defined by

$$C(H_2, H_2, \tau) = T_r\{(\hat{H}_p H_2)\, \hat{S}_0(\tau)\, (\hat{H}_p H_2)\},$$
$$C(H_2; H_1, \tau) = T_r\{(\hat{H}_p H_2)\, \hat{S}_0(\tau)(\hat{H}_p H_1)\}, \tag{23}$$

for which the following relation is valid

$$\int_0^\infty d\tau [C(H_2, H_2, \tau) + C(H_2, H_1, \tau)] = 0$$

We can define new thermodynamic coordinates by

$$\beta_1(t) = \langle H_1 \rangle_t / T_r\{H_1^2\}, \qquad \beta_2(t) = \langle H_2 \rangle_t / T_r\{H_2^2\} \tag{24}$$

which in the high-temperature approximations have the dimension of inverse temperature ($k = 1$). For these formal inverse spin temperatures, the following equation is valid [5]:

$$\frac{\partial \beta_2(t)}{\partial t} = \frac{\beta_1(t) - \beta_2(t)}{T_{IS}} \tag{25}$$

where the cross-relaxation time which characterizes the cross-relaxation process is

$$T_{IS}^{-1} = \frac{-1}{T_r\{H_2^2\}} \int_0^\infty d\tau\; T_r\{(\hat{H}_p H_2) \exp\,[-i(\hat{H}_1 + \hat{H}_2)\tau]\; (\hat{H}_p H_2)\} \tag{26}$$

Using the particular forms of H_1, H_2 and H_p we obtain

$$T_{IS}^{-1} = \frac{1}{2} M_{2,SI} J_z(\Delta\omega_e)$$

where the spectral density function which describe the fluctuations in the thermal bath represented by the abundant spin system are given by

$$J_z(\omega) = \int_0^\infty d\tau \cos \omega\tau C_z(\tau)$$

with $C_z(\tau)$ the dipolar autocorrelation function

$$C_z(\tau) = T_r\left\{\left(\sum_{im} b_{im} I_{iz}\right) \exp\left[\frac{i}{2} \hat{H}_{II}^0 \tau\right] \left(\sum_{i,m} b_{im} I_{iz}\right)\right\} / T_r\left\{\left(\sum_{i,m} b_{im} I_{iz}\right)^2\right\}$$

and $\Delta\omega_e = \omega_{eS} - \bar{\omega}_{eI}$

In eq (27) $M_{2,SI}$ is the Van Vleck second moment of the magnetic-resonance line determined by the cross coupling dipolar interaction

From eq (27) we can observe that maximum cross-polarization rate is obtained for $\bar{\omega}_{eI} = \omega_{eS}$ (Hartmann-Hahn condition) in according with experimental results of Takegoshi and Mc Dowell [4].

4 **Conclusion.** The heteronuclear polarization transfer rate in the case of double resonance time averaged precession frequency have been derived The maximum transfer is obtained for $\Delta\omega_e = 0$ which verify experimental results. [4]. Also have been obtained the variation on T_{IS}^{-1} with $\overline{\omega}_{eI} - \omega_{es}$ as a cross-polarization spectrum

REFERENCES

1. A Pines, M G Gibby and J S Waugh, J Chem Phys **59**, 569 (1973).
2. S R Hartmann and E L Hahn, Phys Rev **128**, 2042 (1962)
3 M Mehring, *Principles of High Resolution NMR in Solids*, 2nd ed (Springer, Berlin, 1983).
4 K Takegoshi and C A McDowell, J Magn Reson **67**, 356 (1986)
5. D E. Demco, J Tegenfeldt and J S Waugh, Phys Rev **B11**, 4133 (1975).

STUDIA UNIV BABEŞ-BOLYAI, PHYSICA, XXXVI, 1, 1991

THE AIR-QUALITY USING TO MEASURE THE BETA-RADIATON FROM AEROSOLS IN CLUJ-NAPOCA

MARTA BAYER*, NICOLETA HIRIŞCĂU*, E. MUNTEANU*

ABSTRACT. The nuclear activity contributes to the radioactive loading of the atmosphere The radioactive materials contained by the air may irradiate the man directly, by inhalation or immersion, or indirectly , through nourisliment chain [2, 3]

The radioactive aerosols are formed by the scattering of the radioactive products in the air, their composition being variable and frequently very complex

This paper presents the obtained result regarding the radioactivity of the aerosols long-lived constituent through ovefall beta measurings

The used working method [1, 8, 9, 10] was based on filtering a definite air volume through F P P and S L F-21-50 with $\varnothing = 3$ cm This was mounted on a plastic or metallic holder and an air pump connected. The filtering lased 7—8 *hours* during this time, a quantity of 25—30 m^3 air was filtered, being absorded by the F P P for aerosols and S F L - 2I-50 for the radioactive gases special filters The total volume of air sempled can be measured The filter is analysed to obtain the integrated radioactivity per unit volume of air By weighing the F P P filter before and after aspiration we can estimate the concentration of powders in air. Before the measuring, the F P P filters were kept in boxes for 3—5 days in order to eliminate the interference of the Rn and Th short-lived products

Table 1

Date of filtering	Volume of air (m^3)	Concentrations of powder ($\mu g/m^3$)	Beta radioactivity after 48 hours (mq/m^3)	
1991				
Jan 20	20 065	26 4	22	±4
Febr 25	24 656	33 3	13	±4
March 10	25 317	406 0	30	±3
March 17	25 248	412 0	24	±4
March 24	25 500	204 0	24	±4
March 31	30 134	206 0	25	±3
April 7	28 034	142 6	31	±4
April 14	27 162	192 2	38	±5
April 21	25 340	343 3	13	±4
May 6	27 002	403 7	20	±4
May 25—26	45 674	374 4	22	±3
June 9—11	76 134	442 6	26	±3
July 8—10	75 490	245 0	18	±3

* *Institute of Public Health and Medical Research Cluj-Napoca*

The radioactivity of the filters was measured by putting them on known fund salvers placed in an anticoincidence counter connected to an impulse-meter.

The reaults are presented in the next table From these F P P for aerosols filter after their measurement of the beta — radiation and I—131 and Cs—137 isotope contents will be determined, black smoke and the others pollute substances and correlation will be searched between these

In the first part of year 1991, the air quality in Cluj-Napoca by overall beta radioactivity and I—131 measurmeent was not worried

REFERENCES

1. * * * — *Caiet metodologic de Igiena Radiaţiilor*, Ministerul Sănătăţii, IISP, Bucureşti, p 77—98, 1981.
2. * * * — *Norme republicane de securitate nucleară Norme republicane de radioprotecţie* C S E.N., Bucureşti, 1976
3. S Milcu — *Radiobiologie* Ed Tehnică, Bucureşti, 1971.
4. O Gimesi, E Bányai Mikrochimica acta (Wien), 1981, **II**, p 313—322
5. Marta Bayer — Proceedings of the Symposium on Methods, Models and Techniqes is Physics and Related Fields, Cluj-Napoca, p 213—214, sept 26—27, 1986
6. Marta Bayer et al. — *Progrese în fizică*, Bucureşti, Măgurele, p 408, 23—24 oct. 1987.
7. M. Oncescu — *Impactul centralelor nucleare asupra biosferei* R B **18.** 1987, febr., I F I N. Măgurele, Bucureşti, 1987
8. J. Losonczi, Maria Lorinc — *Raport KFKI pe anul* 1988; Budapesta, 1989.
9. R.T. Cederwall et al. —Health Physics, vol **59,** nr 5 pp. 533—540.
10. Marta Bayer et al. — Simpozion „Evaluarea stării factorilor de mediu Cerinţe şi soluţii în prezent şi viitor", Timişoara, 3—5 iunie, 1991, vol rezumate pag 57

STUDIA UNIV BABEŞ-BOLYAI, PHYSICA, XXXVI, 1, 1991

BIFURCATIONS AND CHAOS IN A FAMILY OF LOGISTIC MODELS

P. E. STERIAN, I. M. POPESCU*, V. NINULESCU*, O. RANCU*

ABSTRACT. A family of maps of logistic type is presented and analysed The characteristics of such logistic maps are given by a classic analysis of this application Discrete mappings are easier to handle The conclusion is that the simple discrete mappings could have a complicated behaviour, with evolution chaos, but following the universal routes

It is important that the presented applications' family can be known and investigated further

1 **Introduction.** The work deals with a family of one-dimensional discrete mappings

$$x_{t+1} = f(x_t, t_1, r_1, r_2, \ldots, r_n)$$

where x_t characterizes the system at „time" t, f is a differentiable function that applies an interval into itself and $r_1, r_2, \ldots, r_n$ are parameters

Discrete mappings are easier to handle than differential equations which can be integrated by iteration.

Simple discrete mappings can have a very complicated behaviour, with evolution chaos, but following universal routes

2 **The family of logistic models.** Let's consider the simplificated model of a population noninteracting with others We denote by $x(t)$ the number of organisms at time t, the increasing average rate of the population on the interval $[t, t+\tau]$ is

$$r(t, \tau) = \frac{(x(t+\tau) - x(t))/\tau}{x(t) + 0(t, \tau)}, \quad (\lim_{\substack{\tau \to 0 \\ \tau > 0}} 0(t, \tau) = 0)$$

from which

$$r(t) = \lim_{\substack{\tau \to 0 \\ \tau > 0}} r(t, \tau) = \frac{x'(t)}{x(t)}$$

so that

$$x'(t) = r(t)\, x(t)$$

For small populations $r(t) = r_0$ (the static birth rate) and the population is exponentially increasing. When the population became large enough, the competition between organisms can't be ignored and $r(t) < r_0$ We consider Verhulst's effective (dynamic) birth rate

$$r(t) = r_0 - a\, x(t), \quad a > 0$$

* *Polytechnical Institute Bucharest, 79585 Bucharest, Romania.*

The population evolution will be given by the differential equation

$$x'(t) = x(t)(r_0 - ax(t))$$

and — using a linear transformation — by the corresponding discrete mapping

$$x_{t+1} = rx_t(1 - x_t)$$

which is named „logistic".

The family of logistic models is [1]:

(1) $x_{t+1} = rx_t(1 - x_t),\ 0 \leq x_0 \leq 1,\ 0 \leq r \leq 4$

(2) $x_{t+1} = x_t \exp(r(1 - x_t))$

(3) $x_{t+1} = x_t(1 + r(1 - x_t))$

(4) $x_{t+1} = x_t(1 + r(1 - x_t) + (r^2/2)(1 - x_t)^2)$

(5) $x_{t+1} = x_t(1 + r(1 - x_t) + (r^2/2)(1 - x_t)^2 + (r^3/6)(1 - x_t)^3)$

(6) $x_{t+1} = x_t \exp(r(L - x_t)),\quad 0 < L < 1$

(7) $x_{t+1} = rx_t^{1-b}$

(8) $x_{t+1} = x_t(1 - b \ln(rx_t))$

(9) $x_{t+1} = rx_t^{1-b} \exp(-x_t)$

(10) $x_{t+1} = x_t(1 - b \ln(rx_t))\, r^2 \exp(-x_t)$

(11) $x_{t+1} = x_t(1 - b \ln(rx_t))\, r_2(1 - x_t)$

(12) $x_{t+1} = x_t(1 - b \ln(rx_t))\, r_2(1 - x_t - x_t^2/2)$

(13) $x_{t+1} = x_t \exp(r_1 x_t^{m-1} - r_2 x_t^{n-1}),\ r_1, r_2 > 0,\ n > m > 1$

(14) $x_{t+1} = x_t(1 + r_1 x_t^M - r_2 x_t^N),\ r_1, r_2 > 0,\ N > M > 0$

The deriving of models one from each other has been made by Mac Laurin expansion, by transformations and combining parts of other models. The model (3) is reductible to (1) by the linear transformation $x_t \to (r/(r+1))x_t$ and by $r \to r - 1$ As (2) by Mac Laurin expansion and retaining till linear, square or cubic term will give (3), (4) and (5), we reach the relationship between (1) — (5) models. In (6) the linear transformation $x_t \to (1/L)x_t$ implies (2) where $r \to rL < r$

3. Models' characterization

a. Bifurcations diagram and routes to chaos. The study of the models when one of the parameters is varied shows these change from a regular behaviour to an irregular one (chaos in (1)—(6), (8)—(14) models or unbounded evolution (7)).

The typical behaviour is plotted in Fig. 1 where we have considered the model (1) with $0 < x_0 < 1$ and $2{,}8 \leq r \leq 4$. We got it plotting for each

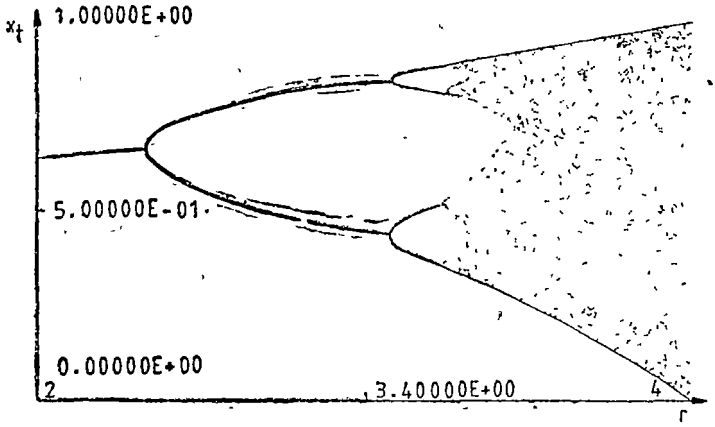

Fig 1

r the iterations from 100 to 150 The first 100 iterations were only computed $x_0 \in (0,1)$ is arbitrarly

The model (1) has two fixed points (solutions of $f(x) = x$ equation) $x_1^* = 0$ stable for $0 \leq r < 1$ and $x_2^* = 1 - 1/r$, stable for $1 < r < 3 = r_1$ When $3 < r \leq 4$ there are no stable fixed points ($|f'(x)| > 1$ for $x =$ fixed point)

We will study the system for these values of r taking the second iterate of f

$$x_{t+1} = f^2(x_t) = r^2(x - (r+1)x^2 + 2rx^3 - rx^4) \quad (f^2 = f \circ f)$$

This has evidently the previous fixed points and in addition the solutions of equation

$$rx^2 - (r+1)x + 1 + 1/r = 0$$

namely

$$x^{*}_{3,4} = (r + 1 \pm \sqrt{(r+1)(r-3)})/(2r)$$

Because we have

$$f^{2\prime}(x_3^*) = f'(x_4^*) = f'(x_3^*)\, f'(x_4^*)$$

the stability of these two points is identical We have

$$f'(x_3^*) = f^{2\prime}(x_4^*) = (f^{2\prime}(x_3^*) + f^{2\prime}(x_4^*))/2 =$$

$$= r^2(1 - (r+1)(x_3^* + x_4^*) + 3r(x_3^{*2} + x_4^{*2}) - 2r(x_3^{*3} + x_4^{*3})) = 1 - (r+1)(r-3)$$

and the stability condition gives

$$r < 1 + \sqrt{6} = r^2$$

With $r \in (r_1, r_2)$, after a sufficiently high number of iterations, the sequence $\{x_n\}_{n \in N}$ settles into a 2-cycle oscillation x_3^*, x_4^*, x_3^*, x_4^* .. So, at $r = r_1 = r$ the system has a period doubling bifurcation

Increasing r beyond r_2, the fourth iterate map f^4 has four stable fixed points in accordance with Figure 1 The bifurcation theory with doubling period was obtained by Mitchell J. Frigenbaum [2] who proved that the system exhibits a sequence of bifurcations at

$$r_1 < r_2 < \ldots < r_\infty = 3{,}569945 \ldots$$

and the sequence $\{r_n\}_{n \in N}$ converges geometrically at a rate

$$\delta = \lim_{n \to \infty} \frac{r_n - r_{n-1}}{r_{n+1} - r_n} = 4{,}669201 \ldots$$

so that with n not large we have

$$r_n \approx r_\infty - C\delta^{-n}$$

For $r > r_\infty$ the system is chaotic

On Figure 1 one can see a ,,window'' in a chaotic region This window is plotted again in Figure 2 on which its limits are clearly noticed.

We explain the ,,window'' — in accordance with Figure 3 — by the existence for the iterate map f^3 besides the fixed points $x_1^* = 0$ and $x_2^* = 1 - 1/r$ of other three pairs of fixed points. Each pair has one stable and one unstable fixed point formed at $r = 1 + \sqrt{8}$, the value of the knob r at which the first bisectrix is tangent in three points at the f^4 diagram.

The bifurcation is named tangent bifurcation. Related with this is Sarkovskii theorem [3] The natural numbers set is written $N = A \cup B$ where $A = \{2^n \quad l \mid n \geqslant 0,\ l \geqslant 3,\ l \text{ odd}\}$ and $B = \{2^m \mid m \geqslant 0\}$ With the order relation on N

$$3 \vdash 5 \vdash 7 \vdash \ldots 2 \cdot 3 \vdash 2 \cdot 5 \vdash \ldots \vdash 2^2 \cdot 3 \vdash \ldots \vdash 2^3 \vdash 2^2 \vdash 2 \vdash 1$$

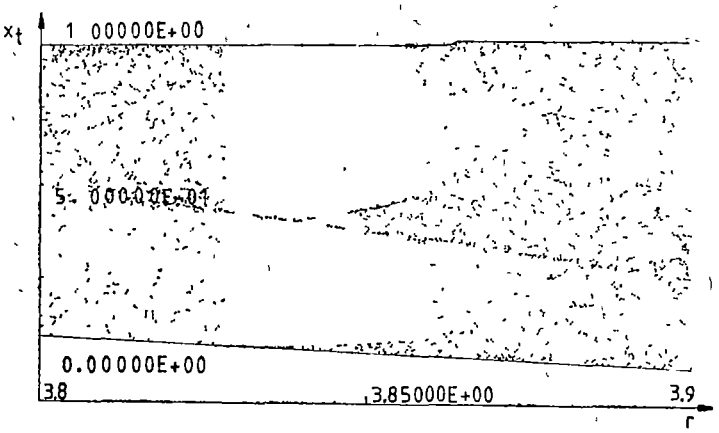

Fig 2

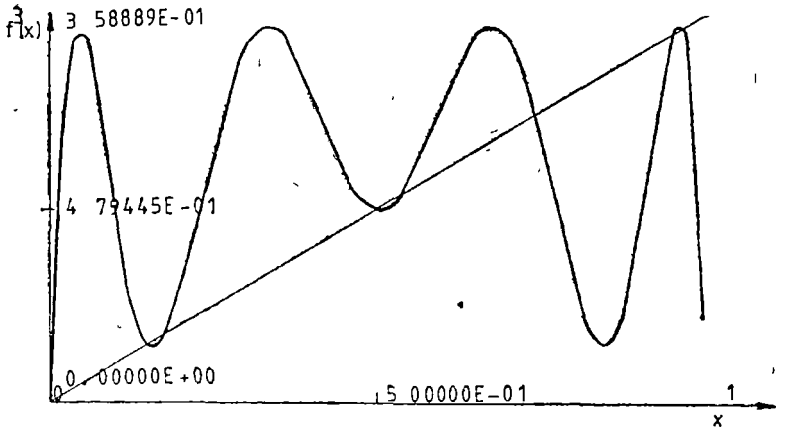

Fig 3

the theorem says that for every T $R \to R$ continous mapping that has a periodic orbit of period n, T has a periodic orbit of period m for every $m \in N$ such that $n \vdash m$

So, the periodic orbit of period 3 implies the existence (for the same value of r) of orbits with arbitrary period Nevertheless, there is no general theorem concerning the stability of periodic orbits In Figure 2 one can see the interval of stability of 3-period orbit and 3 2 bifurcations from the family $3\,2^k (k \in N)$.

Model (7) is a singular case in considered family With $f(x) = rx^{1-b}$, the ‚Schwarzian derivative" [3]

$$Sf(x) = f'''(x)/f'(x) - 3(f''(x)/f'(x))^2/2 = b(1 - b/2)x^{-2}$$

s no negative defined so that the model hasn't the sequence of period — doublings To illustrate system behaviour we suppose $r = 1$ The map has the stable fixed point $x^* = 1$ for $b \in (0,2)$ (Figure 4 a,b) and $\lim_{t\to\infty} x_t = \infty$ for $b > 2$ Figure 4c).

b. Lyapunov's exponent The mappings considered are one-dimensional, so we have only one Lyapunov exponent

$$\chi(r) = \lim_{n\to\infty} \frac{1}{n} \sum_{j=0}^{n-1} \ln |f'(x_j, r)|$$

where $x_j = f(x_{j-1}, r)$ and x_0 is arbitrary in the intervals of the models

Figure 5 shows a typical variation of Lyapunov's exponent for a system that evolves to chaos and is in a good agreement with diagram bifurcations (Figure 1) The values $\chi < 0$ indicate regular behaviour of the system and the existence of some stable periodic orbits, $\chi = 0$ in the bifurcations points and $\chi > 0$ for the chaotic behaviour The route to chaos with P o m e a u — M a n n e v i l l e intermittences is illustrated too, moreover, one can see two k-periodic orbits for $r < 1 + \sqrt{8}$ at which appears the 3-orbit.

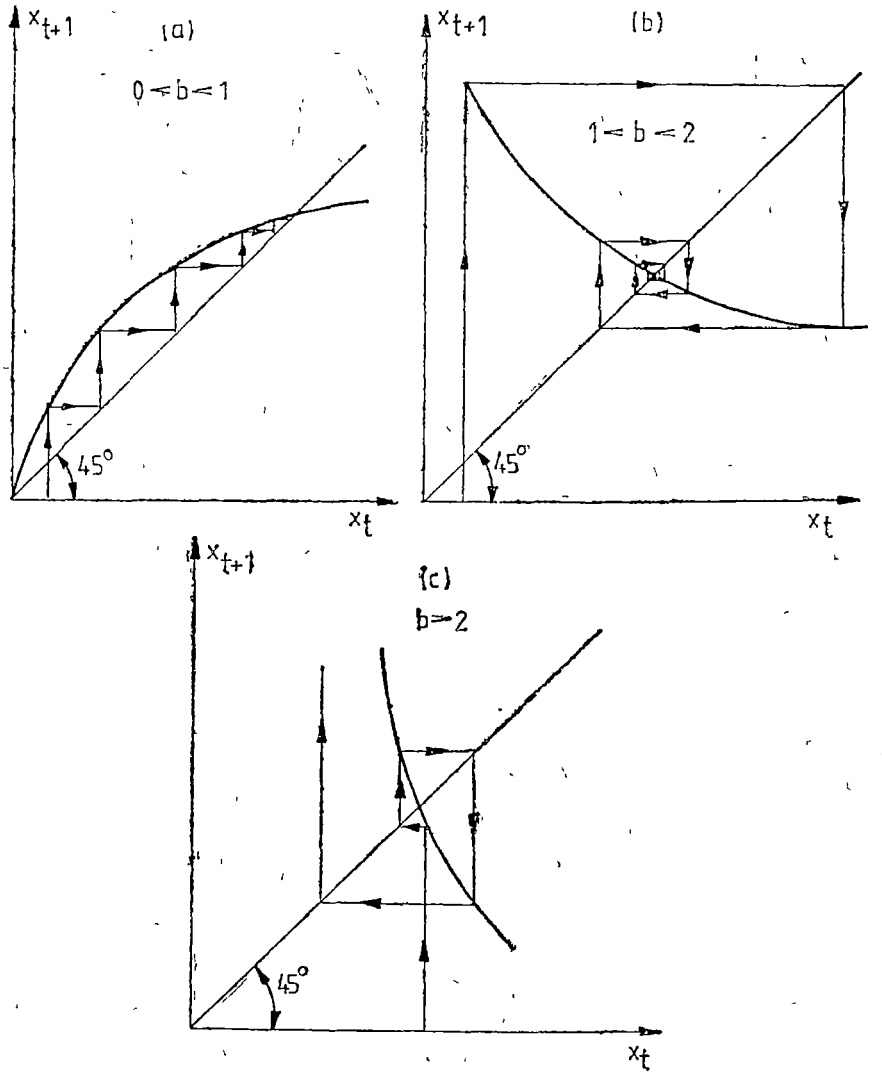

Fig 4.

4. Conclusions, applications.

The study of the family of logistic models emphasizes the similarity in behaviour, the routes to chaos by periodic doubling bifurcations, except model (7), when one of the parameters is varied

The models are used in continuous or discrete forms in economy (inventions, diffusion, forecasting of energy consumptions, in biology (the growth of an organism, demographical problems) etc [1]

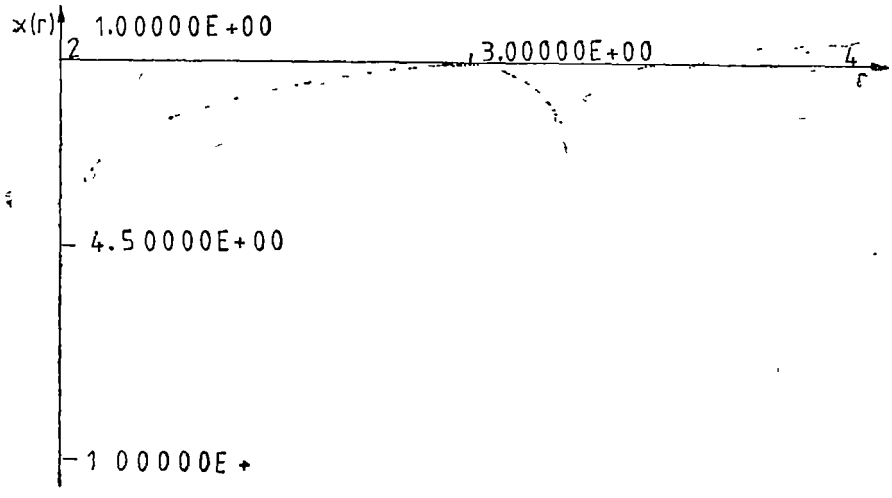

Fig. 5.

REFERENCES

1 Kinnunen, T, Pastijn, H, Revue X (Belgium), nr 4, 1986.
2 M J Feigenbaum, J Stat Phys **19**, 25 (1978)
3. P Stefan, Commun math Phys **54**, 237 (1977)
4. D. Singer, SIAM J Appl Math **35**, 260 (1978)
5. Y Pomeau, P Manneville, Commun Math Phys **74**, 189 (1980).

STUDIA UNIV BABEŞ-BOLYAI, PHYSICA, XXXVI, 1, 1991

NATURAL GEOMETRIC SETTING FOR THE ANTI-BRACKFT

H. BALASIN*, L. TĂTARU**

ABSTRACT. Despite the fact that there is a natural symplectic structure in the Hamiltonian approach even in the extended phase space (1), the corresponding one in the Lagrangian approach is still missing We present a geometric setting for the BRST construction in the Lagragian approach The nature of the anti-bracket operation and its connection to the Schouten-Nijenhuis bracket will be clarified Finally we present an extension of the geometric construction to include the ghost degrees of freedom

1 **Introduction.** A physical system may be described by the space of all trajectories M, where the physical subspace M_c is singled out by the action function $S \in C^\infty(M)$ using the condition $\partial_i S = 0$ In the presence of a gauge group G even M_c contains redundant points That is to say elements of M_c realize the same physical state if they are connected by a gauge transformation. The physical subspace is given by M_c/G and the physical observables become $C^\infty(M_c/G)$ To be definite we assume G to be a Lie group that acts freely on M. That is

$$\begin{aligned}
&\text{group—mapping} && \Phi_g \;\; M \to M && \forall g \in G \\
&\text{orbit—mapping} && \Phi_p \;\; G \to M && \Phi_p(g) = \Phi_g(p) \\
&R_\alpha(p) = \Phi_p'(e) \cdot \sigma_\alpha && \{\sigma_\alpha\} \;. \quad \text{basis of } L(G) \\
&[R_\alpha, R_\beta] = f^\gamma_{\alpha\beta} R_\gamma
\end{aligned}$$

Since it is in general easier to acess functions on M, we need some procedure to identify the physically relevant functions The strategy is to implement the above two step procedure in going from M to M_c and finally to M_c/G in terms of the corresponding C^∞-functions Batalin and Vilkovisky (BV) provided an algebraic construction to implement both steps. [2, 3, 4, 5]
The passage from $C^\infty(M)$ to $C^\infty(M_c)$ is accomplished by noticing that elements of $C^\infty(M_c)$ are in one to one correspondence with elements of $C^\infty(M)$ modulo functions that vanish on M_c The latter are of the form $X^i \partial_i S$ (under some regularity conditions) Using the Koszul resolution of $(C^\infty(M), \{\partial_i S\})$ [5] this may be stated in the form $H^0_\delta(C^\infty(M) \otimes \wedge(V)) = C^\infty(M_c)$, where the following notation has been used

- V is the free vector space generated by elements $\{\Theta^*_i\}$
- δ is the Koszul boundary operator acting on the complex $C^\infty(M) \otimes \wedge(V)$ by its action on the generators

Institut fur Theoretische Physic, Technische Universitat Wien, Wiedner Hauptstraße 8—10, A 1040, Wien, Austria.
* *Univ Babes-Bolyai, Dept of Physics*, 3400 Cluj-Napoca, Romania

$\delta F = 0 \qquad \forall F \in C^\infty(M)$

$\delta \emptyset_i^* = \partial_i S$, which has the property $\delta^2 = 0$

- $H_\delta^p(C^\infty(M) \otimes \wedge(V))$ is the p-th homology space of δ

To achieve the acylicity of δ, which has turned out to be crucial for the existence of the $BRST$-action (see below), BV introduced generated $\{\emptyset_\alpha^*\}$ to kill the cycles $R_i^\alpha \emptyset_i^*$, by imposing $\delta \emptyset_\alpha^* = R_\alpha^i \emptyset_i^*$ ($\emptyset_\alpha^*$ will be identified with a basis of $L(G)$) In order to describe the gauge invariant functions F on M_c, we use the fact that they are anihilated by the generators of the group action (i e $R_x^i \partial_i F = 0$) Using Lie algebra cohomology this may be stated equivalently as $C^\infty(M_c/G) = H_d^0(C^\infty(M_c) \otimes \wedge(L^*(G))$, where we made use of

- $L^*(G)$ the dual of the Lie algebra $L(G)$, where the basis elements will be denoted by $\{c^\alpha\}$,
- d the coboundary operator of the complex $C_\infty(M_c) \otimes \wedge(L^*(G))$ defined on its generators

$dF = c^\alpha R_\alpha^i \partial_i F \qquad \forall f \in C^\infty(M_c)$

$dc^\alpha = \frac{1}{2} f_{\beta\gamma}^\alpha c^\beta c^\gamma$

$d^2 = 0$ because of the Jacobi identity

- $H_d^p(C^\infty(M_c) \otimes \wedge(L^*(G)))$ is the p-th cohomology space of d

Putting the pieces together we find that $C^\infty(M_c/G) = H_d^0(H_\delta^0(C^\infty(M) \otimes \wedge(V)) \otimes \wedge \wedge(L^*(G)))$ BV showed that it is possible identify the latter with the zeroth cohomology of complex H_s^0 of the BRST complex $C^\infty(M) \otimes \wedge(V \oplus L(G) \oplus \oplus L^*(G))$ with coboundary operator given by $s = \delta + d$, with the property $s^2 = 0$ Since s acts as a (graded) derivation on this complex, i e it maps „functions of the BRST complex into „functions", it may be considered as some sort of „vector field". Keeping this and the analogy to the Hamiltonian formalism in mind, BV were able to construct a bracket structure on the $BRST$ complex, the so-called antibracket $(.,.)$ and an element S_{BRST} of the complex that generates the vector field $sF = (F, S_{BRS})$ $\forall F \in C^\infty(M) \otimes \wedge(V \oplus \oplus L(G) \oplus L^*(G))$.

The aim of the present work is to shed some light on the underlying geometry of algebraic BV construction (i e to identify the extended field space and the antibracket as canonical geometric concepts) In a second step we extend the natural structure to incorporate the gauge symmetry of the system Finally we briefly comment on the geometric significance of the $B\ R\ S\ T$ condition singling out physical observables

2 **Batalin-Vilkovisky field space and the Schouten-Nijenhuis bracket.** In order to provide a natural geometric setting for the BV approach and its ingredients, let us first disregard any symmetries that may be present in the system under consideration Therefore we start from a manifold M, which serves as a model for the space of all fields (M will be considered from the sheaf-theoretic point of view. That is to say, the differentiable structure will be defined by assuming M to be a Hausdorff space together with the correspondence $U \to$

$^{\infty}(U)$, for any open $U \subset M$, which defines the smooth functions over U.) ocal coordinates on M will be denoted by $\{\emptyset^i\}$ To set the stage for BV a- proach we consider the supermanifold* M_{ex} that is naturally associated with the ngent-bundle TM of M [14] M_{ex} is obtained by extending the structure eaf C^{∞} of the manifold M to $\wedge\, \mathcal{T}$, where $\mathcal{T}$ denotes the sheaf of sections (TM) of the tangent bundle Local coordinates of TM obtained from $\{\emptyset^i|\}$ e given by $(\emptyset^i, \emptyset^*_j) = (\emptyset^i, \partial_j)$ With respect to these coordinates a function n M_{ex} may be written as

$$f(\emptyset, \emptyset^*) = f(\emptyset) + f^i(\emptyset)\partial_i + \quad : \frac{1}{p!} f^{i_1} \quad {}^{i_p} \partial_{i1} \wedge \quad \cdot\cdot \wedge \partial_{ip} + \ldots,$$

hich may be interpreted as a section of $\mathcal{T}$ Functions with a fixed antighost mber, that is a fixed power of $\emptyset^*_i$, are identified with p-vector fields over Owing to this correspondence we may take advantage of the natural bracket efined on p-vector fields This is the so-called *Schouten—Nijenhuis* (*SN*) *bracket* $[\cdot, \cdot]_{SN}$. [6, 7] In local coordinates it is given by

$$[\ ,\ ] \quad \wedge^p(\mathcal{T}) \times \wedge^q(\mathcal{T}) \to \wedge^{p+q}(\mathcal{T})$$

$$[X, Y] = \frac{1}{(p-1)!q!}(-1)^{p-1} X^{I_p - 1^i} \partial_i Y^{I_q} \partial_{I_{p-1}} \wedge \partial_{I_q} + \qquad (1)$$

$$+ \frac{1}{(q-1)!}\frac{1}{p!}(-1)^{q(p-1)} Y^{I_q - 1^i} \partial_i X^{I_p} \partial_{I_{q-1}} \wedge \partial_{I_p}$$

here

$$X \in \wedge^p(\mathcal{T}),\ Y \in \wedge^q(\mathcal{T})$$

$$\partial_{I_p} = \partial_{i1} \wedge \qquad \wedge \partial_{ip}$$

$$I_p = i_1 \qquad i_P \qquad (2)$$

In the particular case of $p = q = 1$ the SN bracket reduces to the Lie racket Interpreting $\wedge(\mathcal{T})$ as $C^{\infty}(M_{ex})$ we see that the SN bracket defines a linear, odd (since it changes the degree by one) operation on $C^{\infty}(M_{ex})$ The llowing properties of the SN bracket are readily obtained from (1).

- Linearity in both arguments
- Graded commutativity

$$[X,Y] = (-1)^{pq}[Y,X]$$

- Derivation property

$$[X, Y \wedge Z] = [X,Y] \wedge Z + (-1)^{(p-1)q} Y \wedge [X,Z]$$

- Graded Jacobi identity·

$$[X, [Y,Z]] = (-1)^{p-1}[[X,Y], Z] + (-1)^{(p-1)(q+1)}[Y,[X,Z]]$$

for the definition of · supermanifold see the Appendix

(The singnificance of the SN bracket may be seen from the following example Suppose we want to define a Poisson bracket on M using a 2-vector filed h and the definition $\{f, g\} = h^{ij}\partial_i f \partial_j g$ $f, g \in C^\infty(M)$ The condition for $\{\ ,\ \}$ t satisfy the Jacoby identity turns out to be $[h, h]_{SN} = 0$ [8])

This raises the question if there is a connection between the canonical struc ture defined by the SN bracket and the antibracket which is defined [12, 13 for arbitiary functions F, G of $\emptyset$, $\emptyset^*$ in the following manner

$$(F, G) = \frac{\partial_r F}{\partial \emptyset^i} \frac{\partial_l G}{\partial \emptyset^*_i} - \frac{\partial_r F}{\partial \emptyset^*_i} \frac{\partial_l G}{\partial \emptyset^i}$$

Taking F and G to be homogenous of degree p and q in the antifields respecti vely (i e identifying F, G with p, q-vectors) we obtain

$$F = \frac{1}{p!} X^{I_p} \emptyset^*_{i_1} \qquad \emptyset^*_{i_p} = \frac{1}{p!} X^{I_p} \partial_{I_p},$$

$$G = \frac{1}{q!} Y^{I_q} \emptyset^*_{i_1} \qquad \emptyset^*_{i_q} = \frac{1}{q!} Y^{I_q} \partial_{I_q}, \tag{3}$$

$$(F, G) = \frac{1}{p!} \partial_i X^{I_p} \partial_{I_p} \frac{1}{(q-1)!} Y^{iI_{q-1}} \partial_{I_{q-1}} - \frac{1}{(p-1)!} X^{iI_{p-1}} \partial_{I_{p-1}} \frac{1}{q!} \partial_i Y^{iI_q} \partial_{I_q} =$$

$$= (-1)_p [X, Y]^{I_{p+q-1}} \partial_{I_{p+q-1}}.$$

So we have identified the SN bracket, which is a natural object from a differential geometric point of view, up to a power of (-1) with the anti bracket of the BV approach

However, this means that we are in the same position as in the Hamiltonian (BF) approach, which starts from an a priori given symplectic manifold S which provides a Poisson bracket on $C^\infty(S)$ The above considerations show that Lagrangian (BV) approach starts from the supermanifold M_{ex}, which is canonically associated with M together with a skew Poisson structure (or antibracket in physical terminology) on $\wedge \mathcal{F}$ which is given by the SN bracket.

3 Incorporation of Symmetries. Let us now assume that the system under consideration carries the action of a gauge group G More precisely let there be a free right action of G on M. (In this way $G \to M \xrightarrow{\pi} M/G$ becomes a principal fibre bundle) The Killing vector fields relative ot the G-action, which corresponds to a given basis $\{\gamma_\alpha\}$ of the Lie-algebra $L(G)$, will be denoted by $R_\alpha(\emptyset) = R^i_\alpha(\emptyset)\partial_i$ Their commutation relations define the structure constants

$$[R_\alpha, R_\beta] = f^\gamma_{\alpha\beta} R_\gamma$$

Taking into account the previous section shows that we may follow the construction used in the Hamiltonian (BF) approack, which extends the phase space and the Poisson structure to the ghost degrees of freedom Therefore

ur aim has to be the construction of an extension of the canonical superman-
fold $M_{\varepsilon\tau}$ and the SN bracket defined on $C^\infty(M_{\varepsilon\tau})$ in order to accomodate
he ghost degrees of freedom of the BV approach. Guided by the fact that
he ghost are odd degrees of freedom and that they belong to $L^*(G)$, our cons-
ruction will be the following

At first let us define some extension $\hat{M}$ of the original manifold M which incor-
orates the ghosts Obviously $\hat{M}$ has to be a supermanifold. In the next step let
is pass to $T\hat{M}$, which is motivated by the way the previous chapter incorpora-
ed the antifields $\emptyset^*$ Via an appropriate grading let us pass to the $\wedge\hat{\mathfrak{F}}$,
vhich will serve as structure sheaf of $\hat{M}_{\varepsilon\tau}$ Finally by the extension of the SN
racket to $\wedge(\hat{\mathfrak{F}})$ we will obtain the skew Poisson structure on $C^\infty(\hat{M}_{\varepsilon\tau})$.

The construction of $\hat{M}$ is achieved by associating a vector-bundle E with stan-
lard fibre $L^*(G)$ to the principal bundle $G \to M \xrightarrow{\pi} M/G$ This is achieved by
he following construction

$$\begin{aligned} E &= \pi^*(M \times_G L^*(G)) \\ M \times_G L^*(G) &= (M \times L^*(G))/G, \end{aligned} \tag{4}$$

where we take the G-action on $L^*(G)$ to be the coadjoint action, which is defined by

$$(Ad^*(g)\omega,\ \zeta) = (\omega, Ad(g)\zeta) \qquad \forall g \in G \qquad \omega \in L^*(G),\ \zeta \in L(G)$$

Finally we use the projection $M \xrightarrow{\pi} M/G$ to pull back the associated bundle $M \times_G L^*(G)$ to a bundle E over M. Let us now use the bundle E, or more precisely the sheaf of its sections $\varepsilon = \Gamma(E)$ to define the supermanifold $\hat{M}$ to be $(M, \wedge(\varepsilon))$ This object will serve as generalization of M in order to include the ghost degrees of freedom A general element of $C^\infty(M)$ will be of the form

$$f(\emptyset, c) = f(\emptyset) + c^\alpha f_\alpha(\emptyset) + \ \ldots + \frac{1}{p!}\, c^{\alpha_1} \ldots\ c^{\alpha_p} f_{\alpha_1 \ \ldots \ \alpha_p}(\emptyset)$$

with respect to a local coordinate system $(\emptyset^i, c^\alpha)$ In the next step we identify the BV antifields with the tangent vector fields $(\partial_i, \partial_\alpha)$ given by this coordinate system To this end we have to consider the tangent bundle $T\hat{M}$ and the sheaf of its sections $\hat{\mathfrak{F}}$, which is defined to be the set of all derivations of $C^\infty(\hat{M})$. Explicitly, we have

$$\begin{aligned} v \in \mathfrak{F} \Rightarrow v(fg) &= v(f)g + (-1)^{fv} f v(g) \qquad \forall f, g \in C^\infty(\hat{M}) \\ v(\emptyset, c) &= v^i(\emptyset, c)\,\partial_i + v^\alpha(\emptyset, c)\,\partial_\alpha \end{aligned} \tag{5}$$

ith respect to local coordinates $(\emptyset^i, c^\alpha)$.

This construction suggests the definition of $\hat{M}_{ex} = (M, \wedge (\hat{\mathcal{S}}))$, where the exterior product $\wedge$ is taken with respect to the gradation

$$\begin{aligned} v \wedge v' &= (-1)^{(1+v)(1+v')} v' \wedge v \\ &\Rightarrow \partial_i \wedge \partial_j = -\partial_j \wedge \partial_i \\ &\Rightarrow \partial_i \wedge \partial_\alpha = \partial_\alpha \wedge \partial_i \\ &\Rightarrow \partial_\alpha \wedge \partial_\beta = \partial_\beta \wedge \partial_\alpha \end{aligned} \tag{6}$$

The generalization of the SN bracket may be obtained from (1) by simply taking into account the powers of (-1) that arise from pulling the basis of the left term through the components of the right term. The extended SN bracket is therefore conveniently written as

$$\begin{aligned} [X, Y] = (-1)^{X+1} &\left(\frac{1}{(p-1)!} X^{I_{p-1}A} \partial_{I_{p-1}} \right) \wedge \left(\frac{1}{q!} \partial_A Y^{I_q} \partial_{I_q} \right) - \\ &- (-1)^{Y(X+1)} \left(\frac{1}{(q-1)!} Y^{I_{q-1}A} \partial_{I_{q-1}} \right) \wedge \left(\frac{1}{p!} \partial_A X^{I_p} \partial_{I_p} \right), \end{aligned} \tag{7}$$

where the index A denotes either i or α and I is an arbitrary collection of indices. Moreover the relation to the antibracket is given by

$$(X, Y) = (-1)^X [X, Y]$$

The properties of (7) are obviously generalized from the properties of (1) by replacing p with X in the exponent of (-1). Together with the extension of the SN bracket to p-vectors over $\hat{M}$ this construction gives our geometric model of $\hat{M}_{ex}$, the extended field space as a skew Poisson manifold with a skew Poisson structure given by the extended SN bracket.

Appendix.

This section is devoted to the to basic sheaf-theoretic notions used in the theory of supermanifolds. In order to define the concept of a supermanifold [9, 10, 11] it is useful to take a different point of view on an ordinary manifold M. That is, we consider M to be topological space together with an assignment of a ring of continous functions to each open subset U of M (i.e. $U \to \mathcal{A}(U) \subset C(U)$). Moreover the family $\mathcal{A} = (A(U),\ U \subset M \text{ open})$ obeys the following conditions:

- $U \subset V$ open, $f \in \mathcal{A}(V) \Rightarrow f| \in A(U)$
- $V = \bigcup_{\alpha \in I} U_\alpha$ U_α open, I some index set, $g, f \in \mathcal{A}(V)$ and $g|_{U_\alpha} = f|_{U_\alpha}$ $\forall \alpha \in I \Rightarrow f = g$
- $V = \bigcup_{\alpha \in I} U_\alpha$ U_α open, I some index set $f_\alpha \in A(U_\alpha)$ $\forall_\alpha \in I$ s.t.

  $f_\alpha|_{U_\alpha \cap U_\beta} = f_\beta|_{U_\alpha \cap U_\beta}$ $\quad \forall \alpha, \beta \in I \Rightarrow \exists f \in V$ $f|_{U_\alpha} = f_\alpha$
- to every $p \in M$ there is an open neighbourhood $U \subset M$, that is homeomorphic to R^n. Let the components of this homeomorphism be denoted by y^i $U \to R$, then

$$\mathcal{A}(U) := C^\infty(R^n)\,(\times_{i=1}^n (y^i)).$$

Locally the elements of $A(U)$ have the form $f = f(y^1, \ldots, y^n)$.

The first three conditions make the family $\mathcal{A}$ into what is mathematically known as a sheaf. It is called the structure sheaf of M Usually one writes M for the C^∞-manifold instead of the pair $(M, \mathcal{A})$ In the same way one may define a vector bundle E over M by a sheaf ε of free modules over the structure sheaf $\mathcal{A}$ of M ε is identified with the sheaf of sections of the vector bundle E

The passage to a supermanifold is now accomplished by tensoring $\mathcal{A}$ with some exterior product of a vector space V More precisely

$$\text{to every } p \in M \exists U \subset M \text{ open s t } \widehat{\mathcal{A}}(U) \simeq \mathcal{A}(U) \otimes \wedge(V),$$

This defines the extension $\widehat{\mathcal{A}}$ of $\widehat{\mathcal{A}}$ Locally a function in $\widehat{\mathcal{A}}(U)$ becomes

$$f = f(y, c) = f(y^l) + c^\alpha f_\alpha(y^l) + \quad + \frac{1}{p!} c^{\alpha_1} \dots c^{\alpha_p} f_{\alpha_1 \quad \alpha_p},$$

where $\{c^\alpha\}$ denotes a basis of V. Stated differently, a supermanifold is obtained by generalizing the notion of the structure sheaf of an ordinary manifold

A supermanifold $\widehat{M} = (M, \mathcal{A})$ may be constructed by using a vector bundle $V \to E \to M$ over M, and declaring $\widehat{\mathcal{A}} = \wedge(\varepsilon)$, where ε denotes the sheaf of sections of E This construction will mainly be used in our work Using the sheaf-theoretic point of view it is easy to generalize the notion of a vector bundle to a supervector bundle We simply define its sheaf of sections $\widehat{\varepsilon}$ to be a sheaf of free modules over the structure sheaf $\widehat{\mathcal{A}}$ of its base supermanifold $\widehat{M}$ A supervector bundle that is canonically associated with every supermanifold $\widehat{M}$ is the (super) tangent bundle $T\widehat{M}$ It is defined to be the sheaf of all graded derivations $\widehat{\mathcal{S}}$ of $\widehat{\mathcal{A}}$ (Explicitly $v \in \widehat{\mathcal{S}} \Rightarrow v(fg) = v(f\,g) + (-1)^{fv} fv(g) \quad \forall f, g \in \mathcal{A}$) This bundle is locally generated by $\left\{\partial_i = \dfrac{\partial}{\partial y^i}, \partial_\alpha = \dfrac{\partial}{\partial c^\alpha}\right\}$.

Acknowledgement:

One of us (L T) would like to thank Prof W K u m m e r for useful discussions and for the extended hospitality at the Inst fur Theoret Physik, TUW

REFERENCES

1 R L o l l, Comm Math Phys **119** (1988), 509
2 E S. F r a d k i n and G A V i l k o v i s k y, Phys **55 B** (1975) 224
I A B a t a l i n and G A V i l k o v i s k y, Phys Lett **69 B** (1977), 309
3 I A B a t a l i n and G A V i l k o v i s k y, Phys Rev D **28** (1983), 2567
4 M H e n n e a u x, Phys Rep **126** (1985), 1
5 J F i s c h, M H e n n e a u x, J S t a s h e f f and C. T e i t e l b o i m, Comm Math Phys **120** (1989), 379
6 J A S c h o u t e n, *R i c c i C a l c u l u s* (Berlin, 1954)
7 A F r ö l i c h e r and A N i j e n h u i s, Indag Math **18** (1956), 338
8 Y C h o q u e t—B r u h a t, C D e W i t t—M o r e t t e, *Analysis, Manifolds and Physics* Part 2, North—Holland (1989)
9 I A B a t a l i n J Math Phys **22** (1981), 1837
10 S B G i d d i n g s and P N e l s o n, Comm Math Phys **116** (1988) 607
11 B K o s t a n t, Lectures Notes in Mathematics **570** (1975) 177
12 I A B a t a l i n and G A V i l k o v i s k i, J Math Phys **26** (1985), 172
13. M H e n e a u x, Nucl Phys B (Proc Suppl **18A** (1990) 47
14 E W i t t e n, Mod Phys Lett **A5** (1990) 487

Physica fl 1—88 KBM

Tiparul executat la Imprimeria „ARDEALUL“ Cluj, c-da 478.

În cel de al XXXVI-lea an (1991) *Studia Universitatis Babeş—Bolyai* apare în următoarele serii:

matematică (trimestrial)
fizică (semestrial)
chimie (semestrial)
geologie (semestrial)
geografie (semestrial)
biologie (semstrial)
filosofie (semestrial)
sociologie—politologie (semestrial)
psihologie—pedagogie (semestrial)
ştiinţe economice (semestrial)
ştiinţe juridice (semestrial)
istorie (semestrial)
filologie (trimestrial)

In the XXXVI-th year of its publication (1991) *Studia Universitatis Babeş—Bolyai* is issued in the following series:

mathematics (quarterly)
physics (semesterily)
chemistry (semesterily)
geology (semesterily)
geography (semesterily)
biology (semesterily)
phylosophy (semesterily)
sociology—politology (semesterily)
psychology—pedagogy (semesterily)
economic sciences (semesterily)
juridical sciences (semesterily)
history (semesterily)
philology (quarterly)

Dans sa XXXVI-e anné (1991) *Studia Universitatis Babeş—Bolyai* paraît dans les series suivantes:

mathématiques (trimestriellement)
physique (semestriellement)
chimie (semestriaellement)
géologie (semestriellement)
géographie (semestriellement)
biologie (semestriellement)
philosophie (semestriellement)
sociologie—politologie (semestriellement)
psychologie—pédagogie (semestriellement)
sciences économiques (semestriellement)
sciences juridiques (semestriellement)
histoire (semestriellement)
philologie (trimestriellement)